Journal of Materials Chemistry B

ROYAL SOCIETY OF CHEMISTRY

REVIEW

View Article Online
View Journal | View Issue

Cite this: *J. Mater. Chem. B*, 2024, **12**, 4785

Review of NIR-responsive "Smart" carriers for photothermal chemotherapy

Abhijit Karmakar,* Akshay Silswal and Apurba Lal Koner*

Received 20th December 2023,
Accepted 15th April 2024

DOI: 10.1039/d3tb03004k

rsc.li/materials-b

This review focuses on the versatile applications of near-infrared (NIR)-responsive smart carriers in biomedical applications, particularly drug delivery and photothermal chemotherapy. These carriers demonstrate multi-responsive theranostics capabilities, including pH-dependent drug release, targeted delivery of chemotherapeutics, heat-mediated drug release, and photothermal tumor damage. Biological samples are transparent to NIR light with a suitable wavelength, and therefore, NIR light is advantageous for deep-tissue penetration. It also generates sufficient heat in tissue samples, which is beneficial for on-demand NIR-responsive drug delivery *in vivo* systems. The development of biocompatible materials with sufficient NIR light absorption properties and drug-carrying functionality has shown tremendous growth in the last five years. Thus, this review offers insights into the current research development of NIR-responsive materials with therapeutic potential and prospects aimed at overcoming challenges to improve the therapeutic efficacy and safety in the dynamic field of NIR-responsive drug delivery.

1. Introduction

Cancer, a severe pathophysiological threat caused by alterations in inherent cellular processes, has emerged as the second leading cause of death worldwide.[1] Based on the reported data, more than 19.3 million new cancer patients were diagnosed, resulting in approximately 10 million deaths globally in 2020.[2] Moreover, in 2024, only in the United States, 2 001 140 new cancer cases and 611 720 cancer deaths are projected to occur.[3] These emerging reports on cancer accounting for millions of deaths worldwide annually call for the development of potent pharmaceuticals and ensure their targeted delivery. Conventional treatments, *i.e.*, chemotherapy and radiotherapy, for late-stage cancer and adjunct methods for surgery in the early stage are considered ineffective because of their non-specificity and cytotoxicity towards normal cells.[4,5] Nowadays, the major drawback in cancer treatment is the loss of the therapeutic potential of chemotherapeutics due to the failure of sustained and targeted delivery of drugs to tumor sites.[6,7] Furthermore, the persistent use of certain drugs is associated with limitations, including the development of multidrug resistance and emergence of severe side effects, which can lead to death. Consequently, multimodal strategies such as photothermal and photodynamic therapy need to be adopted together with traditional chemotherapy to deal with the rapid spread of this disease. In the case of combined photothermal chemotherapy,

Bionanotechnology Lab, Department of Chemistry, Indian Institute of Science Education and Research Bhopal, Bhopal Bypass Road, Bhauri, Bhopal-462066, Madhya Pradesh, India. E-mail: abhijitkarmakar@iiserb.ac.in, akoner@iiserb.ac.in

Abhijit Karmakar

Dr Abhijit Karmakar obtained his doctoral degree in Chemistry from Visva-Bharati University. During his doctoral research, he was involved in the synthesis and development of novel fluorescent reporters and nanomaterials for probing disease-based cellular biochemical events. His current research is centered on the development of organelle-selective sensors and stimulus-responsive drug-delivery agents.

Akshay Silswal

Dr Akshay Silswal obtained his doctoral degree in Chemistry from IISER Bhopal. During his doctoral research, he was involved in developing fluorogenic molecular rotors for targeting specific cellular organelles to understand their biophysical properties. His current research is centered on the development of novel fluorophores and utilizing them for biomedical applications.

methodically engineered drug delivery systems can simultaneously produce hyperthermia and release drugs in cancer cells, leading to cancer cell death. However, the development of multifunctional drug delivery vehicles is a complex process and associated with numerous challenges in various stages, each demanding advanced scientific knowledge, particularly in the field of cancer.[8,9] Thus, in response to these challenges, researchers are exploring innovative approaches, such as leveraging drug delivery systems and prodrugs.[7,10,11] Stimulus-responsive delivery systems offer a promising avenue for achieving precision drug delivery.[12] This not only enhances therapeutic efficacy but also minimizes the risk of nonspecific toxicity associated with conventional treatments. Light, serving as an on-demand external stimulus, has emerged as a particularly advantageous tool in the realm of photoresponsive drug and gene delivery systems.[13] Its unique properties, including spatiotemporal precision, safety, and minimal interference with cellular signaling networks, make it an attractive option. This has led to the development of sophisticated photoresponsive systems that allow for site-specific cargo release through the precise control of light irradiation parameters.

In recent research, the combination of photoresponsive delivery materials with photothermal therapy and other stimulus-responsiveness has demonstrated potential efficacy in achieving precise control and programmed regulation of drug release.[14–16] This has paved the way for exploring multi-responsive theranostic applications, particularly in the context of cancer treatment. In this aspect, NIR-light responsive materials have shown great promise for photothermal therapy and the on-demand delivery of chemotherapeutics. NIR light is advantageous compared to visible light due to its transparent and deep-tissue penetration capability, lower tissue absorption, and reduced scattering.[11,17] A broad NIR window is available, which can be classified as NIR-I (wavelength range of 750–900 nm) and NIR-II (1000–1700 nm).[18] Thus, light in the NIR region has been widely explored by researchers given that it allows deeper tissue penetration, greater tissue tolerance and higher photothermal conversion efficiency than UV and visible light.[18,19]

Apurba Lal Koner

Dr Apurba Lal Koner is an associate professor in the Department of Chemistry in IISER Bhopal. One of his current research interests lies in the design and synthesis of novel fluorescent reporters for live-cell fluorescence imaging for understanding sub-cellular properties.

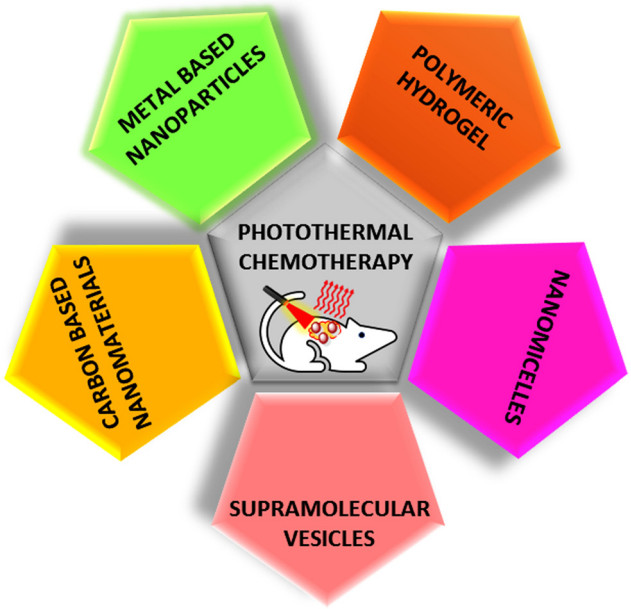

Fig. 1 Schematic presentation of different classes of NIR-responsive materials for photothermal chemotherapy.

In this review, we have discussed the emerging and biocompatible NIR-responsive drug delivery systems such as metal-based, carbon-based, polymeric, and soft-nano materials. The different classes of NIR-responsive materials based on photothermal chemotherapy are schematically represented in Fig. 1. This comprehensive review highlights the recent advancements in this field, and also provides insights into the prospects of developing near-infrared-responsive drug delivery systems. These systems show promise for significantly enhancing the efficacy of drugs, while ensuring precision in drug delivery, marking a crucial stride forward in the ongoing efforts to combat challenging diseases such as cancer.

2. NIR-responsive nanomaterials

2.1 Carbon-based nanomaterials

In the last few years, carbon-based nanomaterials (CBNs) have created a remarkable impression among researchers due to their theranostic applications such as bioimaging, biosensing, drug/gene delivery, photothermal, and photodynamic therapy.[20,21] The family of CBNs consists of an abundance of materials of different dimensions with distinctive features such as fullerenes, carbon nanotubes (CNTs), graphene-based derivatives, and carbon-based quantum dots (CQDs).[22,23] Due to their high surface area and polyaromatic rings, these CBNs can carry chemotherapeutics on their surface either through non-covalent interactions, *e.g.*, π–π stacking interactions and van-der Waals interactions, or specific covalent modifications.[24] Moreover, CBNs possess tremendous NIR light-absorbing properties and high photoconversion efficiencies, making them effective for the photothermal therapy.[25] In addition, the strong light absorption rate and lipophilicity of these carbon-based

nanomaterials can enhance the cell permeability, which proves their suitability for diagnosis and treatment.[26]

Among the CBNs, carbon nanotubes (CNTs) have attracted special attention owing to their unique physical and chemical properties.[27–29] The needle-like shape of CNTs facilitates their escape from abnormally leaky tumor blood vessels and easy penetration through the cell membrane by the "nanoneedle" mechanism.[30] In addition, CNTs, especially multi-walled-CNTs (MWCNTs) have strong absorptivity towards both NIR windows (700–1400 nm), which can be utilized in photothermal therapy.[31]

In 2018, Yi and co-workers exploited multi-walled carbon nanotubes (MWCNTs) as a drug-delivery system for the delivery of tamoxifen (TAM), an antiestrogenic agent, to enhance its therapeutic effects (as shown in Fig. 2).[32] They utilized lentinan (LEN), a β-1,3 β-glucan with β-1,6 branches, a type of natural polysaccharide, as a dispersant, which also increased the cellular uptake of MWCNTs (MWCNTs–TAM–LEN). Irradiation using an 808 nm (NIR-I) laser increased the apoptotic rate in MCF-7 cells from 23.43% to 78.11% compared to without irradiation. The hyperthermia effect of MWCNTs–TAM–LEN resulted from its capacity for photothermal conversion. Moreover, the synergistic interplay between the photothermal effect of MWCNTs–TAM–LEN and the cytotoxic impact of TAM amplified the cytotoxicity within cancer cells. The results indicated that the combination of photothermal therapy and chemotherapy provides a selective approach to eliminate cancer cells and enhance antitumor effects.

Similarly, Roxbury and colleagues self-assembled DNA-wrapped single-walled carbon nanotubes (DNA-SWCNTs) with model drug (FITC-Dex)-containing liposomes, and further embedded them in a 3D hydrogel for the purpose of developing a photo-responsive drug release device within the NIR-II window.[33] Negatively charged DNA-functionalized SWCNTs were electrostatically attracted to the positively charged lipids. The photothermal efficiency of CNT was validated by the temperature reaching 46 °C upon NIR laser exposure at 1122 nm after the first 60 s laser pulse. Moreover, the NIR light-mediated slow release of drugs was also observed in this system.

Graphene-based 2D nanomaterials especially graphene oxide (GO) and reduced graphene oxide (rGO) are valuable systems for drug delivery applications due to their high surface area, planar sheet-like structure and presence of abundant oxygen functionalities for hosting drug molecules.[34,35] Moreover, these nanomaterials are easy to functionalize and their surface can be modified according to the targets. Researchers often functionalize GO with PEG for the delivery of chemotherapeutics given that PEGlyated GO systems show enhancement of aqueous solubility, biocompatibility, drug loading efficacy, and induce stability in drug delivery systems in the blood compartment compared to only GO.[34,36–38] In the past few years, PEGylated graphene oxide (GO-PEG) has also been used for the efficient photothermal ablation of tumors in animal experiments, owing to its high optical absorption in the near-infrared (NIR) region.[39–41] Mauro and co-workers demonstrated the use of a folic acid-conjugated PEGylated graphene oxide nanocomposite in the photo-thermal delivery of anticancer agent doxorubicin (DOX) hydrochloride.[42] This GO-based nanocomposite could incorporate a high amount of DOX (>33.3% w/w) and release its 100% of its payload in 300 s under NIR-I exposure (810 nm) with a low power density (0.2 W cm^{-2}), which indicates the high photoconversion efficiency of the GO–PEG–Fol/DOX system. In comparison to free DOX, the potency of GO–PEG–Fol/DOX remarkably increased after NIR exposure (IC_{50} from 8.69 to 0.51 μM and from >10 to 1.88 μM for MCF7 and MDA-MB-231, respectively).

In this context, Peng *et al.* also utilized PEGlyated GO surface functionalized with folic acid (FA) for the two-stage NIR-mediated cancer treatment of tumor-bearing mice.[43] At first, the GO nanocomposite (GO–PEG–FA) was internalized in adipose derived stem cells (ADSCs) to target the breast tumor effectively through the blood circulation. ADSCs exhibited affinity towards the tumor tissue with intrinsic tumor-tropism

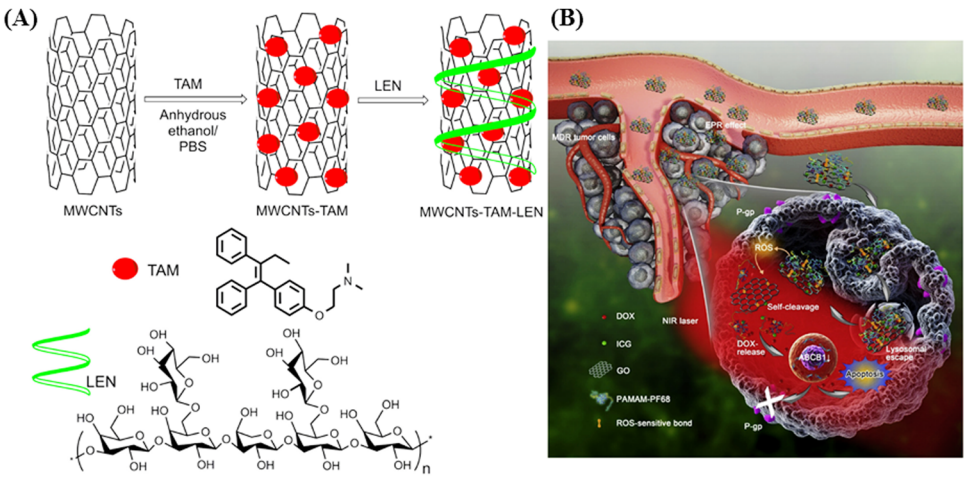

Fig. 2 Schematic illustration of (A) MWCNTs–TAM–LEN and (B) intravenously applied NIR light-responsive nanocomposite for overcoming tumor multidrug resistance. Reproduced with permission from ref. 32 Copyright 2018, Elsevier.

behavior *via* an inflammatory gradient.[44] Then, in the first stage of NIR radiation, ADSCs were disrupted for the slow release of GO–PEG–FA and folic acid receptor-specific delivery inside the tumor cells. Subsequently, second-stage NIR radiation was applied for photothermal therapy to destroy the malignant cells, where the GO-based nanocomposite efficiently generated heat. In the *in vitro* condition under 808 nm (NIR-I) light irradiation, the maximum temperature of the GO–PEG–FA-laden ADSCs increased, reaching 42.6 °C after 8 min from 38.2 °C, which indicates the high photothermal conversion efficiency of PEGlyated GO (as shown in Fig. 3A and B). Moreover, further modification of GO–PEG–FA with ADSCs was proved to be effective, given that almost 88% tumor inhibition was achieved in the 44-day treated mice in comparison to the GO–PEG–FA-treated group, where an inhibition efficiency of only 32% was observed.

Gao and colleagues developed absorbent graphene oxide (GO) and polyamidoamine-Pluronic F68 (PPF68) *via* diselenide bonds, and encapsulated the NIR photosensitizer indocyanine green (ICG) and chemotherapeutic drug DOX *via* π–π stacking and hydrophobic interaction.[45] They characterized the conjugation of graphene oxide with PPF68 by monitoring the change in the stretching frequencies at 1735 and 1628 cm^{-1}, which are assigned to the C═O stretching vibrations in the –COOH groups, that at 1646 cm^{-1}, corresponding to C═O in –CO–NH–, and the stretching vibrational frequency of C–N and bending vibration of N–H of the secondary amide group (1547 cm^{-1}) *via* FTIR spectroscopy. The researchers observed a monolayer of prepared graphene oxide (GO) using AFM. The drug was encapsulated through a combination of π–π stacking and hydrophobic interactions. The size of the nanocomposite expanded as a result of the step-by-step loading of the drug. The ICG/GO-PPF68 matrix remained relatively photostable and biocompatible within the NIR-I window. ICG/DOX/GO-PP68 inhibited the growth and proliferation of MCF-7/ADR cells efficiently by taking advantage of the synergistic effects of chemotherapy and PTT. These NIR-responsive versatile nanocomposites were demonstrated to successfully treat multidrug-resistant tumor cancers *in vivo*.

Li *et al.* explored the tremendous capability of Pluronic F127 micelle-stabilized graphene (GO) as a photoresponsive nanodrug delivery vehicle for combined chemo-photothermal therapy.[46] The anticancer drug DOX was bound through non-covalent interactions due to the presence of abundant oxygen functionalities on the surface of GO as well as sp^2 hybridized planar structure. The Pluronic F127 (F127) micelles endowed the nanovehicle with water solubility and sustained drug-release characteristics, whereas excellent NIR light to heat conversion efficiency of GO facilitated NIR-laser mediated drug release within the tumor cells. This F127-GO hybrid hydrogel

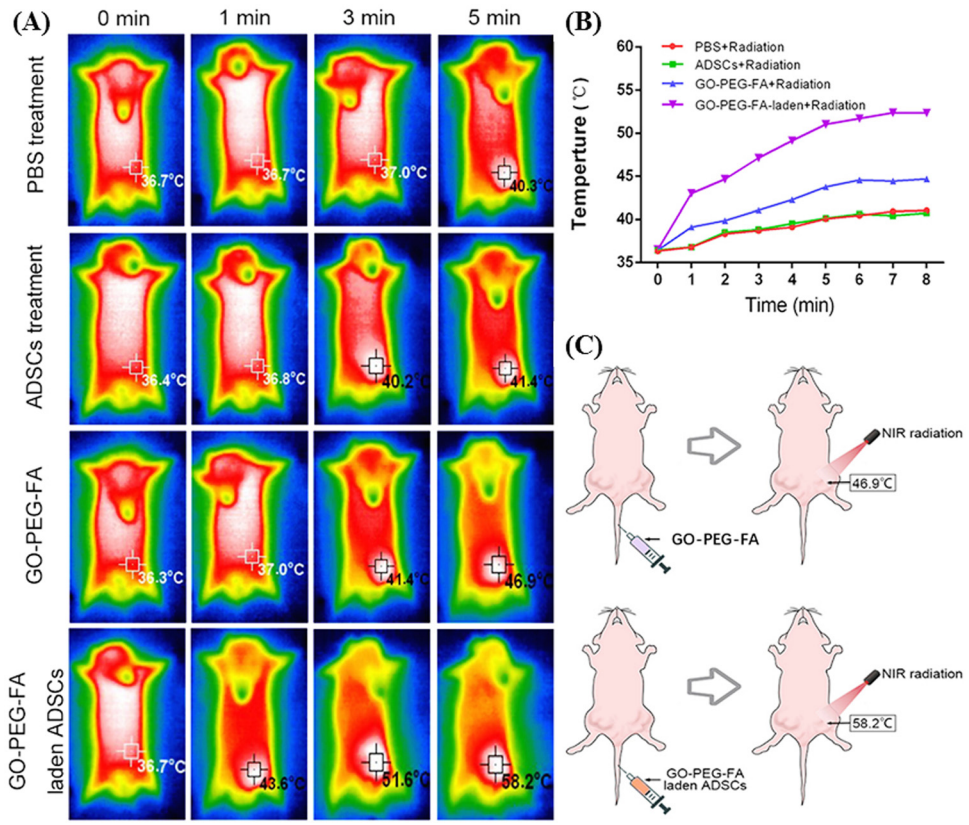

Fig. 3 *In vivo* photothermal assay: (A) *in vivo* thermal images of the tumor site after treatment with NIR radiation. (B) Temperature profile of tumor sites in mice in each group after NIR radiation treatment. (C) Maximum temperature reached at the tumor site after NIR irradiation in mice after injection of GO–PEG–FA or GO–PEG–FA-laden ADSCs *via* their tail vein. Reproduced from ref. 43 Copyright 2023, Taylor & Francis.

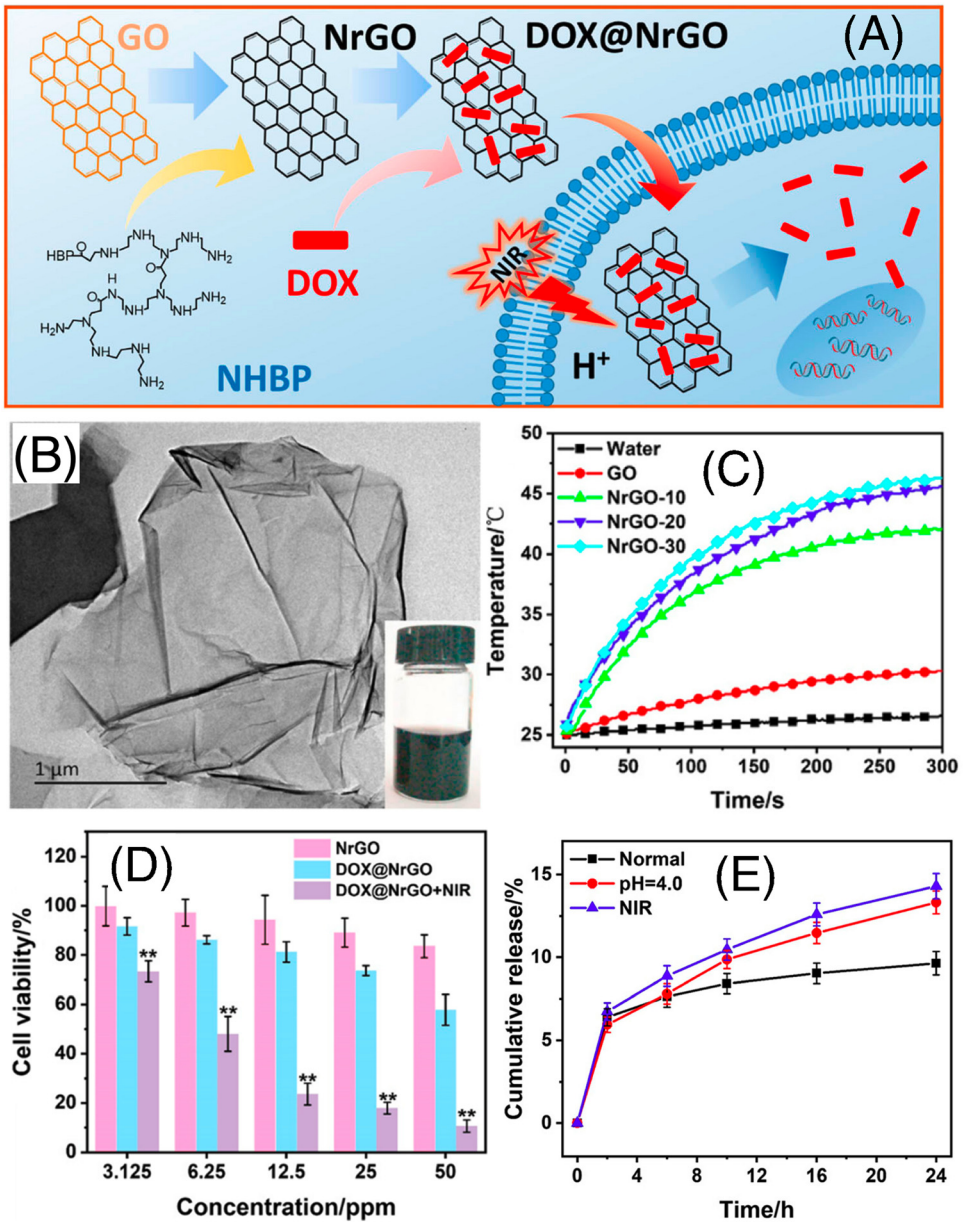

Fig. 4 (A) Schematic illustration of the preparation and chemo-photothermal therapy of DOX@NrGO. (B) TEM image of NrGO; inset shows the optical photograph of the corresponding sample. (C) Heating curves of NrGO-30 at different laser power densities under 808 nm irradiation, (D) tumor cell inhibition investigation of DOX@NrGO with different treatments, and (E) *in vitro* drug release profiles of DOX@NrGO under various conditions. Reproduced with permission from ref. 47 Copyright 2018, Springer.

exhibited an effective DOX loading efficiency of up to 100% and retarded the tumor progression in tumor-bearing mice upon 808 nm (NIR-I) laser irradiation. Dai and co-workers successfully designed and synthesized hydrophilic NrGO by performing a simple reaction of GO and amino-terminated hyperbranched polymer (NHBP) (as shown in Fig. 4A).[47] This material was thoroughly characterized using various spectroscopic and microscopic techniques (Fig. 4B and C, respectively). The synthesized NrGO exhibited good biocompatibility and outstanding photothermal property (as shown in Fig. 4D). Later, NrGO was used for the delivery of the anticancer drug DOX using pH and light. Its release property was shown to be accelerated at low pH value and NIR-I irradiation (as shown in Fig. 4E). Thus, these dual-responsive materials are advantageous for chemo-photothermal synergistic therapy.

Lim and co-workers investigated a 3D printable nanohybrid scaffold with multiple functionalities, which was comprised of gelatin methacryloyl (GelMA) and polyphenolic carbon quantum dots (CQDs), for endogenous tissue repair and therapy, specifically focusing on bone tissue.[48] The CQDs were synthesized using a wet chemistry method and the bioactive molecule phloroglucinol (1,3,5-trihydroxybenzene). These bioactive CQDs served as a photothermal source material for drug delivery and subsequent therapy for osteosarcoma. By

irradiating the hydrogel with 808 nm (NIR-I) light at a power density of 1.0 W cm^{-2}, the temperature of the hydrogel rapidly increased from 25 °C to 75 °C within 6 min. The 3D printed GelMA-Y scaffold, loaded with chemotherapeutic drugs (DOX and PTX), was employed for photothermal therapy. It was hypothesized that the GelMA-Y@DOX scaffold alone lacked the capability to generate reactive oxygen species (ROS) but could produce a significant amount of singlet oxygen radicals upon NIR irradiation. This property could be harnessed for hyperthermia-triggered osteosarcoma therapy. Due to the excellent drug delivery properties of the GelMA-Y scaffold, the GelMA-Y@DOX scaffold was explored in an *in vitro* anti-osteosarcoma study in MG-63 cells. The 3D printed GelMA-Y scaffold is considered a smart delivery vehicle, leveraging the controlled photothermal properties of Y-CQDs for the sustained release of water-soluble chemotherapeutic drugs, such as DOX.

Wang and co-workers reported the combined use of both chemo and photothermal therapies with biocompatible and monodispersed hollow carbon nanospheres (HCNs).[49] Due to its mesoporous nature with a large pore volume, HCN has the capability to fit hydrophobic drugs through hydrophobic and π–π stacking interactions. HCN exhibited 59.06% loading efficiency for the anticancer drug paclitaxel, which is much higher than that of mesoporous silica. Upon near-infrared (NIR-I) laser illumination, HCN effectively converted absorbed light into heat, which triggered the release of the anticancer agent by detaching the binding interactions between HCN and the paclitaxel molecules. After 24 h, 29.3% and 19.5% of paclitaxel was released with and without the NIR laser, respectively. HCN also showed significant antitumor efficacy with NIR light-induced photothermal damage as well as paclitaxel release in HCT 116 cells.

Researchers have also fused carbon-based systems with other nanomaterials to harness the near-infrared (NIR-II)-responsive photothermal capabilities of carbon quantum dots (NIR-II-CQDs).[50,51] The hybridization of black phosphorus nanosheets with CQDs resulted in remarkable photothermal conversion efficiencies in both the NIR-I (77.3%) and NIR-II (61.4%) windows, surpassing that of pristine BP (49.5% and 28.4% at 808 nm and 1064 nm, respectively).[52] In this context, Liu *et al.* demonstrated *in vivo* tumor ablation by mannose-modified aluminum-doped carbon quantum dots (M/A-CQDs) through the photothermal strategy in the NIR-I window.[53] Furthermore, the development of multifunctional nanozymes and combining them with carbon-based nanomaterials such as carbon dots is also a promising approach for photothermal chemotherapy. Wang *et al.* developed an NIR-II-responsive (1064 nm laser irradiation) photothermal-enhanced nanocatalytic therapy (NCT) platform, leveraging CQD@Co_3O_4 heterojunctions.[54] This innovative approach involved the deposition of NIR-II-responsive CQDs on the surface of Co_3O_4 nanozymes, resulting in a synergistic therapeutic effect.

Polydopamine (PDA) has been extensively applied in various biomedical fields, serving as an imaging contrast agent, antioxidants, UV protectant, and agent for photothermal therapy. Its versatility arises from its biocompatibility and ability to chelate metal ions, scavenge free radicals, and absorb a wide spectrum of light. However, its relatively low photothermal efficiency remains a challenge that necessitates improvement. Deng and team innovatively enhanced the near-infrared (NIR) absorption of carbon quantum dots by introducing them on the surface of polydopamine (PDA-PEI@N,S-CQDs), offering a promising solution to the above-mentioned issue.[55] Remarkably, despite the mere conjugation of 4% (w/w) of CQDs on the surface of PDA, there was a notable 30% increase in photothermal efficiency. Additionally, PDA-PEI@N,S-CQDs demonstrated versatility as a drug carrier, accommodating up to 60% (w/w) of DOX and enabling stimulus-responsive drug release triggered by the lysosomal pH (pH 5.0) and 808 nm (NIR-I) laser irradiation. Zhao *et al.* utilized mesoporous hollow carbon nanospheres (HCN) for photothermal chemotherapy in the NIR-II window.[56] They conjugated hollow carbon nanospheres with polymer CD-PGEA [consisting of one β-cyclodextrin core (CD) and two cationic ethanolamine-functionalized poly(glycidyl methacrylate) (PGEA) arms] and utilized this system for drug/gene delivery with NIR-II (1064 nm, 0.5 W cm^{-2}, 5 min) irradiation.

Although widespread research is being conducted on carbon-based stimulus-responsive systems, there are still some disadvantages related to the physicochemical properties of these nanomaterials. The toxicity of carbon-based materials is a major issue given that clinical trials proved that they can deposit within cells and tissues.[57] Additionally, certain carbon nanomaterials exhibit slow degradation rates within the body, which can potentially lead to long-term accumulation and adverse effects.[58] The surface chemistry of carbon nanomaterials can be challenging to control, limiting the ability to functionalize them for specific biomedical applications.[59] In the field of biomedicine, carbon-based nanomaterials present significant potential. However, it is imperative to address their drawbacks diligently to guarantee their seamless and safe integration into clinical applications.

2.2 Metal nanomaterials

Nowadays, gold nanoparticles (AuNPs) with different morphologies are being widely used for NIR-mediated photothermal therapy among various precious metal nanomaterials.[60–62] It has been reported that gold nanoshells and nanorods with a large size (50–150 nm) absorb better in the NIR region than the small-size AuNPs.[63] Owing to the localized surface-plasmon resonance (LSPR) band of AuNPs, the collective oscillation of electrons can resonate with the incident NIR light and AuNPs can effectively promote the conversion of light energy to thermal energy.[64] The LSPR band of gold nanorods (AuNRs) is located in the NIR region, making them preferable candidates than gold nanospheres for NIR light-mediated photothermal therapy.[65] Furthermore, the electrons of gold nanostructures are initially distributed over the conduction band levels and with light irradiation they oscillate and become polarizable. These excited free electrons become a stream of hot electrons with the resonance of external fields and relaxes *via*

phonon emission on the scale of a few picoseconds, leading to an increase in temperature in the environment by tens of degrees Celsius.[66] Researchers are also exploiting the NIR-absorbing properties of AuNPs by integrating them with anticancer drugs and thermo-responsive linkers for the delivery of chemotherapeutics as well as in photothermal tumor ablation.[67–69]

In one study, Deinavizadeh *et al.* demonstrated combined photothermal chemotherapy based on NIR-responsive gold nanorod (AuNR)-functionalized β-cyclodextrin nanosponges.[70] PEGylated gold nanorods were encapsulated in the pores of β-cyclodextrin-based nanosponges (β-CD NS) to prepare the AuNR-S-PEG.β-CD NS nanocomposite for further loading of DOX molecules. The maximum drug loading efficiency was found to be 35 wt%. At neutral pH, *i.e.*, 7.4, due to the solubility issue of DOX, only 13% of the total loaded DOX was released after 24 h, whereas at pH 5.5, the drug release increased to 20%. At higher pH, the OH groups of the nanosponges were protonated and the electrostatic interaction between the nanosponges and DOX molecules weakened. This phenomenon also indicates the pH-responsive drug release behaviour of the nanocomposite. Under irradiation of an 808 nm (NIR-I) light source and at pH 5.5, the % DOX release was further enhanced to 92% after 24 h, which indicates the higher photothermal conversion efficiency by the gold nanorods (AuNRs). In the presence of NIR irradiation, the DOX-conjugated AuNR-S-PEG.β-CD NS composite exhibited enhanced A549 cellular cytotoxicity. Moreover, AuNR-S-PEG.β-CD NS alone showed an increase in temperature in the culture media up to 47 °C upon NIR irradiation for 5 min, which is sufficient to damage cancer cells.

The NIR-responsive photoconversion efficacy of gold nanorods was also utilized by the Akhter group for chemo-photothermal therapy. In this work, they coated gold nanorods with polyelectrolyte poly(sodium-4-styrenesulfonate) (PSS) and utilized them for loading of DOX.[71] The drug loading capacity of PSS-GNRs was determined to be approximately 76%. Upon NIR-I irradiation at 808 nm (1.5 W cm^{-2}) for 2 min, the cumulative release of DOX was observed to be nearly 40% at pH 5, in contrast with 22% from the non-irradiated sample. Moreover, this nanocomposite exhibited photothermal efficiency by increasing the temperature of the media by 52 °C and 45 °C without DOX and with loaded DOX, respectively. The cell cytotoxicity studies revealed that the DOX-loaded nanocomposite exhibited increased cell death, reaching 93% under NIR irradiation compared to 65% without laser exposure and 84% for DOX alone.

Park and collaborators engineered a nitric oxide-releasing thermos-susceptible nitrogel (NO-GEL) to deliver immune modulatory agents deeply into tumors, dealing with the challenges associated with synergistic cancer immunotherapy.[72] The hydrogels, which were composed of hyaluronic acid (HA) and Pluronic F127, were integrated with gold nanostars (GNSs), an indoleamine 2,3-dioxygenase (IDO) inhibitor (NLG919), a stimulator of interferon gene (STING) agonist (DMXAA), and cysteine-NO (Cys-NO) for the localized delivery of small water-insoluble molecules. This delivery was accomplished through *in situ* injection or implantation, aiming to optimize the drug concentrations within tumors and minimize the toxicity to healthy tissues. The inclusion of GNSs in NO-GEL enhanced the heat dissipation in local tumors, and near-infrared (NIR-I) laser irradiation (808 nm) triggered the release of nitric oxide (NO). This triggered the release of NO, effectively depleted tumor collagens and degraded the dense extracellular matrix, facilitating the homogeneous and deep delivery of NLG919 in the tumors. Additionally, the elevated expression of IDO in the immunosuppressive tumor microenvironment and photothermal therapy (PTT)-induced increase in IDO expression were addressed. The sustained delivery of NLG919 downregulated the local IDO expression, which was upregulated during PTT. This downregulation promoted the survival and infiltration of cytotoxic $CD8^+$ T cells in the tumors. The PTT-mediated thermal ablation induced immunogenic cell death, resulting in the release of numerous tumor antigens captured by antigen-presenting cells.

DMXAA released from NO-GEL, in combination with PTT, activated the STING pathway, leading to the release of type-I interferon (IFN-I) and other proinflammatory chemokines, thereby evoking an antitumor immune response. The photothermal chemotherapy of NO-GEL is schematically depicted in Scheme 1. The efficacy of NO-GEL was investigated in both *in vitro* and *in vivo* systems, specifically studying its antitumor effects in a 4T1 mouse tumor model.

Sofla *et al.* coated gold nanorods (AuNRs) with a pH-sensitive thiol-ended amphiphilic triblock copolymer (PAA-*b*-PDMAEMAQ-*b*-PCL-SH) for combined photothermal and chemotherapy.[73] The anticancer agent methotrexate (MTX) was loaded in the nanocomposite and under NIR-II light irradiation of 1064 nm for 4 min, the synthesized AuNRs@polymer exhibited photothermal drug release. In chemo-photothermal therapy, the cell viability decreased by up to 19.69% when MCF7 cells were treated with AuNRs@polymer-MTX, which was significantly lower than chemotherapy alone (AuNRs@polymer-MTX: 55.21%) or photothermal therapy alone (AuNRs@polymer + laser: 62.12%).

Zhu *et al.* developed a photothermal chemotherapy-based combined system with NIR-responsive gold nanorod-curcumin conjugate.[74] Herein, curcumin was covalently attached to 11-mercaptoundecanoic acid (MUA) and cetyltrimethylammonium bromide (CTAB) functionalities, which were exchanged from the surface of Au NRs. Mice were intravenously injected with identical doses of MUA-curcumin conjugates, AuNR@PEG or Au NR@curcumin and PBS, respectively. Both AuNR-based nanocomposites were administered to tumor-bearing mice and after 24 h tumor sites were irradiated with an 808 nm (NIR-I) laser (0.95 W cm^{-2}) for 10 min. The AuNR@curcumin conjugate exhibited effective suppression of tumor growth. Alternatively, NIR irradiation helped to attain focal hyperthermia environment as well as cleavage of the esterase bonds between MUA and curcumin for its on demand release.

Zhang and co-workers engineered an NIR-responsive thermosensitive hydrogel system with chitosan/hydroxypropyl

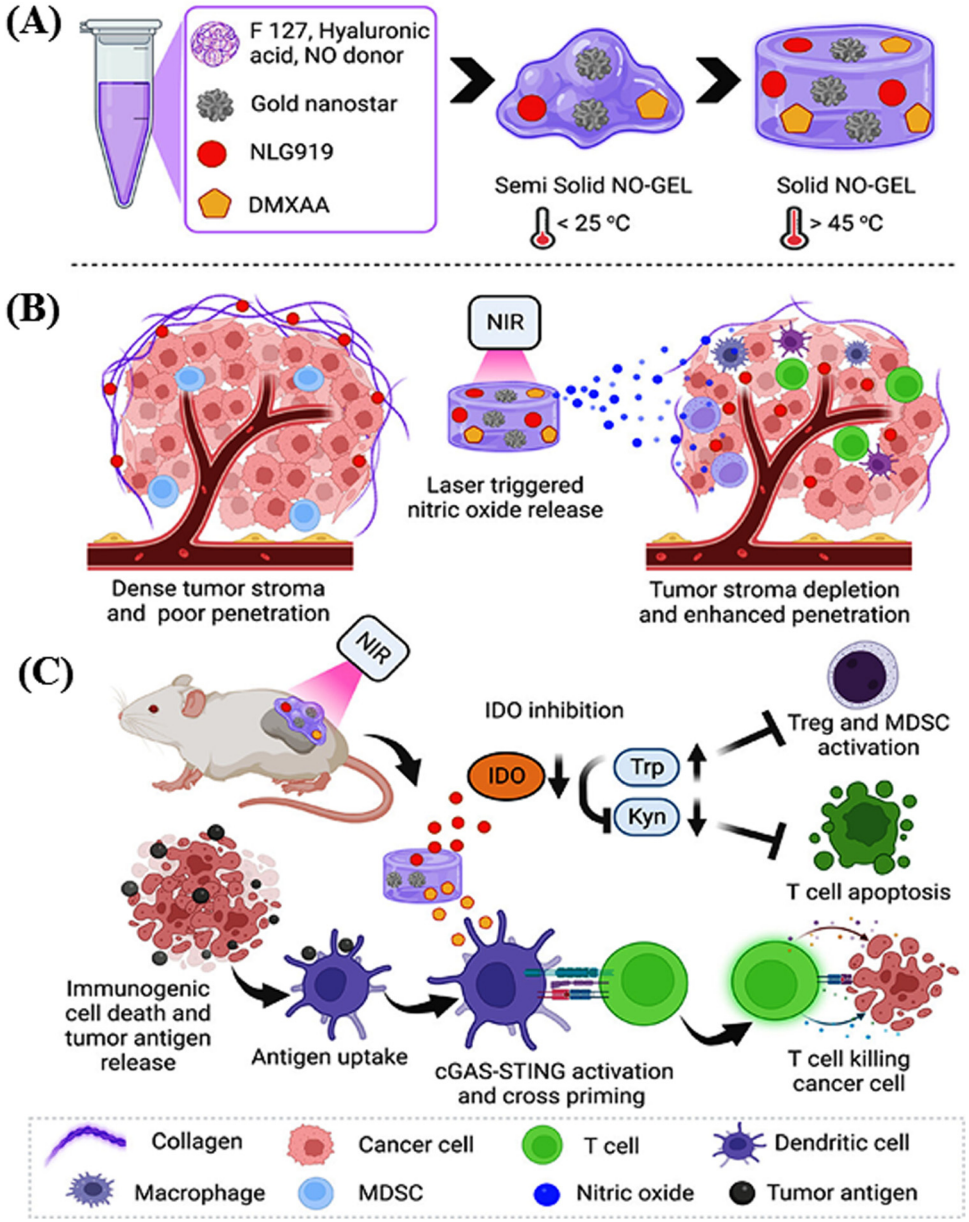

Scheme 1 Schematic presentation of the formation of NO-GEL for enhanced photothermal immunotherapy (A). Reduction of the tumor stroma and enhanced penetration by *in situ* laser-triggered NO release (B). Modulation of antigen and T cell activation by the sustained release of DMXAA and apoptosis of suppressed T cells by NO-GEL in combination with DMXAA through photothermal therapy (C). Reproduced with permission from ref. 72 Copyright 2023, the American Chemical Society.

cellulose (CS/HPC) composite network integrating polydopamine (PDA)-modified Fe_3O_4 nanoparticles.[61] Upon 808 nm NIR-I laser irradiation, the Fe_3O_4@PDA nanoparticles achieved higher photothermal conversion efficiency (η) (48.9%), and as a result weakened the hydrogen bond or charge interaction between nanoparticles and DOX. Furthermore, the hyperthermic conditions resulted in the disruption of crosslinks and rapid release of DOX inside the tumor cells. The synergistic effect of DOX and NIR laser irradiation led to nearly complete eradication of A549 and HeLa tumor cells, with survivability percentages of only 10.8% and 8.3% respectively. These values were substantially lower than that observed for photothermal therapy (PTT) or chemotherapy alone, as illustrated in Fig. 5.

Gao and colleagues introduced a chemo-photothermal synergistic drug delivery system comprised of gold nanoshell-coated wedelolactone liposomes (AuNS-Wed-Lip) designed for tumor cell targeting.[75] In this drug delivery system, wedelolactone liposome and gold-nanoshell were linked by L-cysteine, which was shown to be an effective nanocarrier for antitumor drug delivery, on demand drug release, and photothermal therapy under NIR-I light irradiation. It was capable of absorbing 780–850 nm NIR-I light and converting light energy to heat

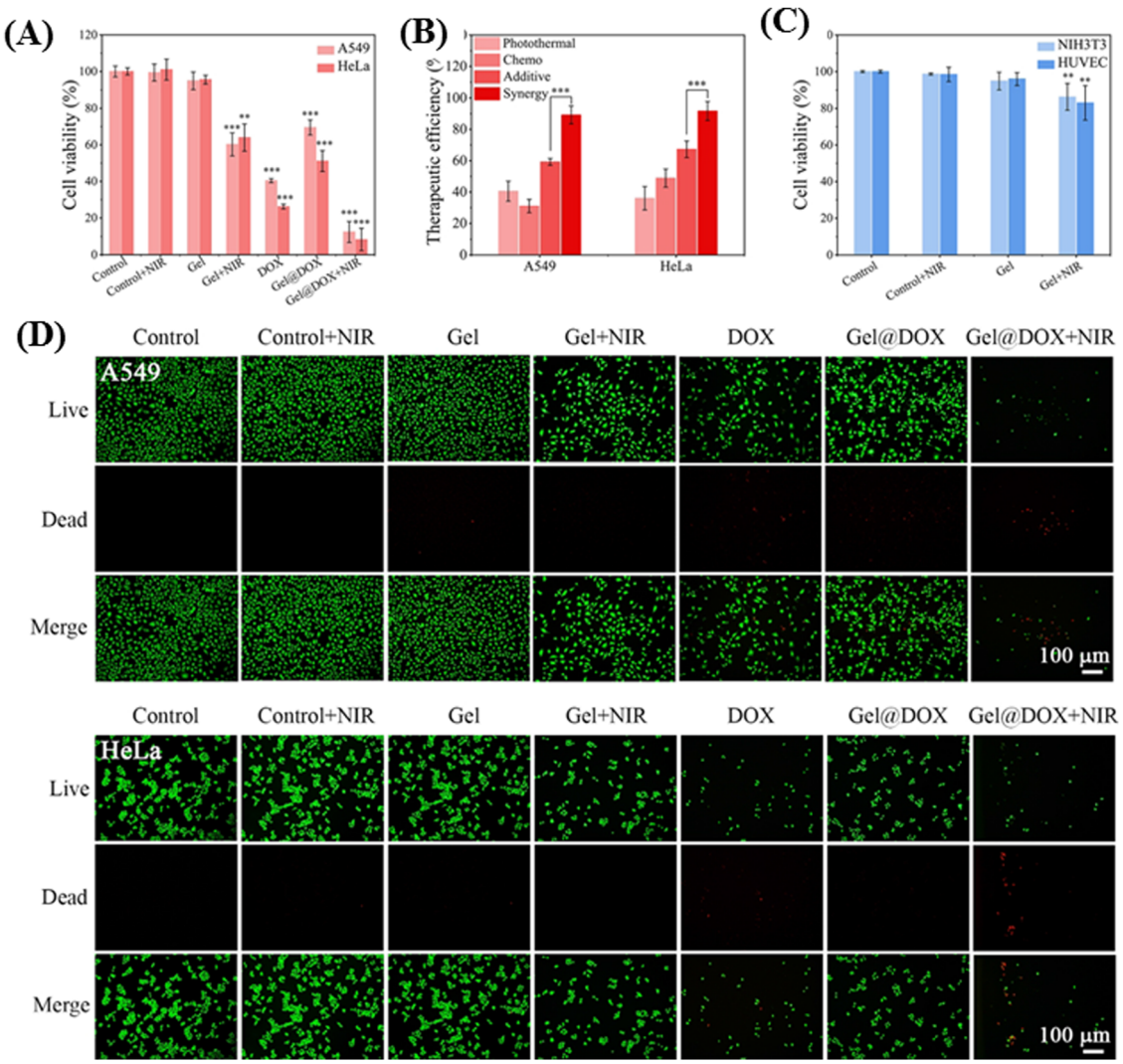

Fig. 5 (A) Cell viability of tumor cells (A549 and HeLa) after exposure to various treatments (control ± NIR, gel ± NIR, DOX, Gel@DOX ± NIR; NIR irradiation: 1 W cm^{-2}, 10 min) and continued culture for 24 h. (B) Therapeutic efficiencies of photothermal, chemo, additive and synergistic therapy. (C) Cell viability of normal cells (NIH3T3 and HUVEC) after exposure to the same hyperthermia environment (control ± NIR, Gel ± NIR; NIR irradiation: 1 W cm^{-2}, 10 min) and continued culture for 24 h (compared with the control group, ** and *** indicate statistically significant difference calculated by two-sample *t*-test). (D) Live/dead co-staining images of tumor cells (A549, HeLa) after various treatments. Reproduced with permission from ref. 61 Copyright 2022, Elsevier.

rapidly. Hyperthermia promoted wedelolactone release rapidly from the system. Under NIR irradiation, the release of AuNS-Wed-Lip reached up to 97.34% over 8 h, demonstrating effective on-demand drug release. Furthermore, a notable inhibition rate of up to 95.73% for 143B tumor cells was observed with AuNS-Wed-Lip upon laser irradiation (refer to Fig. 6A). This outstanding inhibition efficacy translated to *in vivo* antitumor studies with S180 tumor-bearing mice (see Fig. 6B–D). The results underscored the chemo-photothermal synergistic effect achieved by AuNS-Wed-Lip as an antitumor drug delivery system, highlighting its promising potential in cancer therapy.

Sun *et al.* reported the development of the NIR-II activable nanoplatform termed AuSi@FePB, which was designed for synergistic ferroptosis therapy and photothermal therapy.[76] The fabrication of the AuSi@FePB nanoplatform involved coating a polydopamine shell coordinated with iron (Fe-PDA) on silica-encapsulated gold nanochains (AuNCs@SiO_2), with the GSH synthesis inhibitor L-BSO incorporated on the surface of Fe-PDA. NIR-II photoirradiation-induced local heating not only efficiently triggered photothermal therapy (PTT) but also notably amplified the Fenton reaction, resulting in the production of reactive oxygen species (ROS) and depletion of glutathione (GSH). Due to the overexpression of glutathione in cancer cells, the glutathione-driven release of MnO_2 and chitosan-capped hollow gold nanorods (AuHNR@MnO_2@CS) was observed to occur specifically in cancer cells in a target-specific manner.[77] An advantage of this system lies in its ability to execute simultaneous actions, such as photothermal therapy by AuHNR upon NIR-II irradiation and chemodynamic therapy by Mn^{2+}. Recent advancements in tumor therapy emphasize the

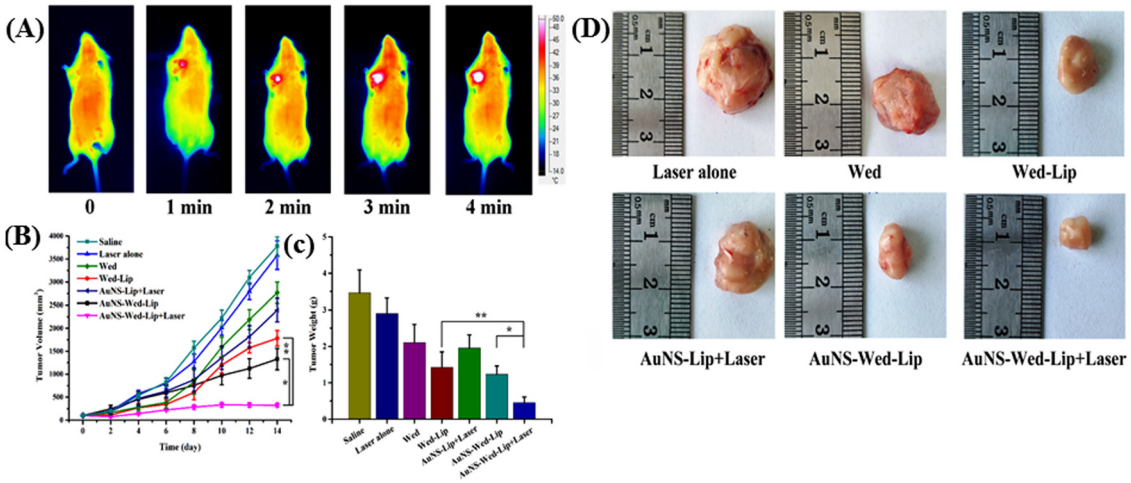

Fig. 6 (A) Thermal images of S180 tumor-bearing mice exposed to NIR irradiation after injecting AuNS-Wed-Lip. (B) Tumor volume changes in tumor-bearing mice in different groups. (C) Tumor weights of mice in different groups. (D) Photographs of the tumors removed from the mice bearing S180 tumor at day 14. Reproduced with permission from ref. 75 Copyright 2019, Elsevier.

importance of multimodal therapeutic approaches for enhanced efficacy such as image-guided photothermal chemotherapy.[78–80] Before initiating therapy, the solid tumor can be accurately visualized by using nanoparticle-based imaging techniques for precise diagnosis. Among the various nanoparticle-enhanced imaging technologies, surface-enhanced Raman spectroscopy (SERS) has shown remarkable potential for ultrasensitive biological imaging.[81,82] Yin *et al.* developed a multifunctional theranostic nanoplatform referred to as RGD–pAS@AuNC.[83] This platform consisted of mesoporous silica-coated gold nanostars with a cyclic Arg–Gly–Asp (RGD)-coated gold nano-cluster shell. Notably, it significantly enhanced the surface-enhanced Raman spectroscopy (SERS) signals and improved the near-infrared NIR-II-induced photothermal therapy and photoresponsive DOX delivery. Similarly, NIR-II-activable and biotin-decorated hollow gold nanoshells were also used as cancer cell-specific, dual-modal imaging-guided photothermal and radio-sensitizing therapy toward breast cancer.[84] Cheng *et al.* demonstrated radionuclide ^{131}I-labeled gold nanoframeworks (^{131}I-AuNFs) for radiotherapy-combined NIR-II-triggered PTT of breast cancer.[85] Under NIR-II laser irradiation (1064 nm), the tumor growth in mice injected with AuNFs was inhibited by 57.8%, while in the mice injected with ^{131}I-AuNFs, it was completely inhibited (100%). Researchers have also used the bioorthogonal click reaction-triggered release of the cancer pro-drug lonidamine for enhanced cancer photothermal therapy with PEGlyated gold nanoparticles in the NIR-I regime.[86] Due to the increased intracellular ROS levels in cancer cells, an alternative option is to employ the ROS-responsive sustained release of gold nanoparticles for photothermal therapy in the NIR-I window.[87] Li and co-workers showcased a comprehensive phototheranostic platform, employing near-infrared II (NIR-II) dual-plasmonic Au@Cu_{2-x}Se core–shell nanocrystals (dpGCS NCs). This innovative platform integrated photoacoustic (PA) and photothermal (PT) imaging, facilitating chemodynamic therapy (CDT), photocatalytic therapy (PCT), and photothermal therapy (PTT).[88] Remarkably, all these functionalities were activated by a single NIR-II laser.

2.2.1 Upconversion nanoparticle. Various studies have explored the application of upconversion nanoparticles (UCNPs) in diverse biomedical contexts, showcasing their versatility and potential impact. Zhu and colleagues utilized a pH low insertion peptide (pHLIP) to enhance the cancer-targeting properties of UCNP-based photodynamic therapy (PDT), minimizing overheating effects and improving the treatment efficiency.[89] Li and co-workers developed a stimulus-responsive nanoplatform (UCSSDH) for PDT, integrating near-infrared (NIR) light-triggered drug release with tumor microenvironment activation. This system achieved burst drug release and effective cancer cell targeting, addressing challenges such as off-target effects and poor tissue penetration.[90] In another study, UCNP-based platforms were engineered for photo-controlled chondrogenic differentiation of mesenchymal stem cells (MSCs) *in vivo*, offering potential applications in regenerative medicine. The UCNP nanoplatform enabled the control of cell differentiation and long-term tracking of MSCs using NIR light.[91] Moreover, a photoresponsive UCNP nanoplatform was designed for near-infrared light-mediated control of intracellular drug release to regulate the osteogenic differentiation of MSCs, with potential applications in osteoporosis therapy.[92] Cerruti and co-workers developed upconverted nanoparticles coated with photocleavable hydrogels for controlled drug delivery and deep tissue imaging, offering opportunities for tissue engineering, biomapping, and cellular imaging applications.[93] These studies demonstrate the multifaceted capabilities of UCNP-based platforms in addressing challenges in cancer therapy, regenerative medicine, and drug delivery, paving the way for innovative biomedical applications.

Despite the specific benefits of nanomaterials, including their small size and large surface area, which enhance the reactivity with biological targets, toxic effects are still possible.

Consumer and industrial products utilizing nanotechnology are confronted with a range of safety and sustainability concerns.[94] Numerous problems regarding the safety and long-term sustainability of consumer and industrial goods based on nanotechnology remain unresolved.[95] Moreover, the aggregation of metal-based nanoparticles in the body is an issue for their clinical applications.

2.3 Metal-free nanomaterials

This section discusses various nanocarriers, including conventional liposomes, polymeric micelles, proteins, inorganic nanomaterial-based vehicles, and carriers such as cell-derived vectors, nanogels, and hybrid nanosystems. Hybrid nanosystems, combining different nanomaterials, are highlighted for their potential in cancer treatment, given that they can leverage the advantages of individual components in one system. Polymeric self-assemblies, specifically vesicles and micelles constructed from amphiphilic copolymers, are emphasized as promising chemotherapeutic nanocarriers. The unique nanostructures of their shell–core design enable the encapsulation of hydrophobic drugs within the micellar cores. Simultaneously, their hydrophilic coronas serve to shield the entrapped therapeutics in the core, protecting them from the external biological environment during blood circulation. However, challenges such as stability after drug encapsulation and structural integrity limit the effectiveness of polymeric micelles. Factors such as high dilution and shear stress can lead to the premature release of therapeutics after intravenous injection, given that micelles may dissociate below their critical micelle concentration. Here, we present the recent reports exploring the synergistic potential of combining chemotherapy and photothermal therapy to address these challenges.

Liu and team explored anticancer drug DOX-loaded PEG functionalized black phosphorus quantum dots (BPQDs) for combined photodynamic, photothermal and chemotherapy.[96] Folic acid was linked with PEG to enable the receptor-specific delivery of the anticancer drug-loaded BPQDs into cancer cells. Upon NIR laser irradiation, BPQDs generated a high flux of reactive oxygen species (ROS) and heat, leading to the release of DOX and causing damage to tumor cells. Under NIR-I irradiation at 808 nm (2 W cm^{-2}), intravenous injection of the nanocomposite increased the temperature to 56.8 °C at the tumor site of tumor-bearing mice.

Xue *et al.* reported the synthesis of an NIR-I responsive nanocomposite with the combination of gelatin-PCL (GP) substrate and multifunctional black phosphorus nanosheets (BPNSs) for wound healing after melanoma surgery.[97] Initially, they conjugated the BP nanosheets with polyethylene glycol (PEG) and functionalized them with folic acid (FA) prior to loading of DOX. Subsequently, the whole nanosystem (BP@DOX/PEG-FA) was conjugated with GP substrate through co-electrospinning. Upon NIR irradiation with an 808 nm laser, the gelatin scaffold exhibited a sol–gel transition due to the photothermal effect and released the BP-based nanoformulation (BP@DOX/PEG-FA) for internalization within melanoma cells. BPNSs enhanced the tissue repairing process by activating the ERK1/2 and PI3K/Akt pathways and the DOX molecules were detached from the nanocomposite and exhibited a chemotherapeutic effect. The maximum release of DOX was found to be 87.4% within the melanoma cells at the laser power density of 0.85 W cm^{-2}.

Li *et al.* formulated combined polymeric nanomicelles based on PT@MFH for NIR-responsive photothermal activity and delivery of the chemotherapeutic drug paclitaxel (PTX).[98] The nanomicelles were prepared from an amphiphilic block

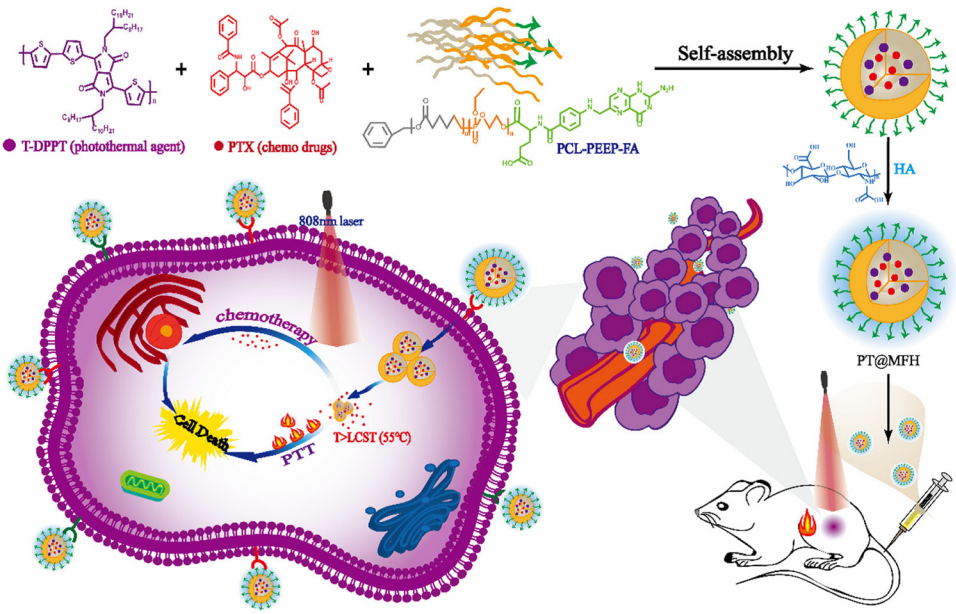

Scheme 2 Schematic illustration of PT@MFH for targeted tumor photothermal chemotherapy. Reproduced with permission from ref. 98 Copyright 2022, the Royal Society of Chemistry.

copolymer (PCL-PEEP) and a photothermal polymer (T-DPPT) and paclitaxel (PTX) were encapsulated within the cavities of the nanomicelles (as shown in Scheme 2). Moreover, the nanomicelle surface was decorated with folic acid and hyaluronic acid for cancer cell receptor-specific delivery. The T-DPPT moiety exhibited exceptional photothermal conversion efficiency of up to ~70% upon 808 nm laser (NIR-I) irradiation, which was effective in the generation of local hyperthermic environment to tumor cells as well as sustained PTX release.

Manna and co-workers demonstrated an interesting result of the NIR-I-light-mediated cleavage of *o*-nitrobenzyl containing an 11-membered macrocyclic Gemini cationic amphiphile (Fig. 7A).[99] The macrocycle was decorated with a 12-carbon-long alkyl chain linker (nIR12), which led to the conversion of the spherical to a nanotubular self-assembly in the aqueous solution (Fig. 7B). The 2-nitrobenzyl group appended with nIR12 acted as an NIR light-absorbing moiety and the energy was depleted by opening the constrained ring to an open-chain conformation *via* easy cleavage of the C–O bond through the Norrish type II mechanism. This amphiphile exhibited low cytotoxicity. Later, the successful entrapment of the anticancer drug DOX and its NIR-I light triggered release (Fig. 7C and D) and delivery to cancerous MDA-MB-231 cells was demonstrated. This NIR-light-mediated transformation of assemblies can be utilized for various applications in photodynamic therapy.

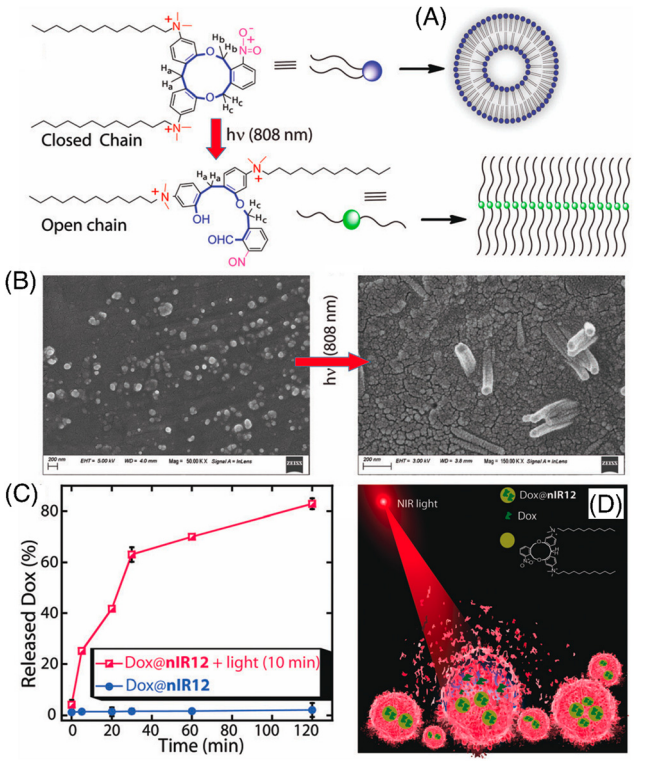

Fig. 7 (A) NIR-light-induced modulation of self-aggregation patterns of nIR12, (B) FESEM images of water-soluble aggregates of nIR12 before and after 10 min of NIR-light treatment, (C) effect of NIR-light treatment on the DOX release kinetics of nIR12 at pH 7.4, and (D) cartoon diagram representing NIR-light treated DOX release. Reproduced with permission from ref. 99 Copyright 2021, The Royal society of Chemistry.

In this context, Zhang and colleagues developed a multi-responsive, *i.e.*, pH and NIR light, liposomal system based on Cypate-BTSL and poly(methacryloyl sulfadimethoxine) for photothermal activity and chemotherapeutic delivery.[100] DOX was encapsulated within cationic liposomes containing Cypate, NIR-I responsive bubble-generating thermosensitive BTSL and NH_4HCO_3 (as shown in Fig. 8A). Subsequently, the whole system was integrated with pH-sensitive poly(methacryloyl sulfadimethoxine) (PSD) through non-covalent interaction. Under slightly acidic pH condition near the tumor site (pH 6.5), PSD was deshielded and the liposomes showed charge reversal capability and further released the DOX molecules (as shown in Fig. 8B).

Moreover, under NIR irradiation, the higher photothermal conversion efficiency of Cypate induced hyperthermia to produce CO_2 bubbles by decomposing NH_4HCO_3, which further facilitated rapid drug release. Especially at pH 5.0, the cumulative release of DOX from PSD/DOX/Cypate-BTSL was 87.8% in 1 h (as shown in Fig. 8C).

Recently, there have been reports of image-guided multimodal cancer therapies using liposomes in the NIR-II region.[101] Du *et al.* introduced a novel nanomedicine termed PATSL for fluorescence imaging in the NIR-II and combinatorial therapy of glioblastoma. PATSL incorporated temperature-sensitive liposome (TSL) carriers, NIR-II-emissive molecule, and photothermal aggregation-induced emission (AIE) dyes [electron-acceptor moiety benzobisthiadiazole (BBT) conjugated with electron-donor molecule *N*,*N*-diphenyl-4-(1,2,2-triphenylvinyl)aniline (DPTPEA)], together with the chemotherapeutic agent paclitaxel (PTX).[102] The combination of photodynamic therapy with photothermal therapy is a wise choice to overcome the low intercellular oxygen level, paving the way for the development of multifunctional strategies in cancer biology. Li *et al.* developed a dual strategy focusing on endoplasmic reticulum (ER)-targeting photodynamic therapy (PDT), photothermal therapy (PTT), and immunotherapy.[103] Their nanosystem was comprised of ER-targeting pardaxin (FAL) peptide-modified hollow gold nanospheres conjugated with indocyanine green (ICG) (FAL-ICG-HAuNS), in addition to an oxygen-delivering hemoglobin (Hb) liposome (FAL-Hb lipo), designed to counteract hypoxia. Under NIR-I irradiation, their nanosystem increased the singlet oxygen level ($^1O_2$) in cells and induced significant ER stress, resulting in the exposure of calreticulin (CRT), a substance for immunogenic cell death (ICD) on the cell surface compared to non-targeting nanosystems. Ni and co-worker demonstrated pH-responsive, NIR-II dye-conjugated lipid nanoparticles for enhancing the mRNA delivery efficiency in a stimulus-responsive photothermal-promoted endosomal escape delivery (SPEED) strategy.[104] Under 1064 nm laser irradiation, their system achieved 50.2% photothermal conversion efficiency.

Liposome-based injectable hydrogels offer distinct advantages, including prolonged drug delivery, high drug loading efficiency, and low systemic toxicity.[105] Kong *et al.* introduced a thermosensitive liposomal hydrogel for NIR-II-responsive photothermal chemotherapy of pancreatic cancer.[106] Their

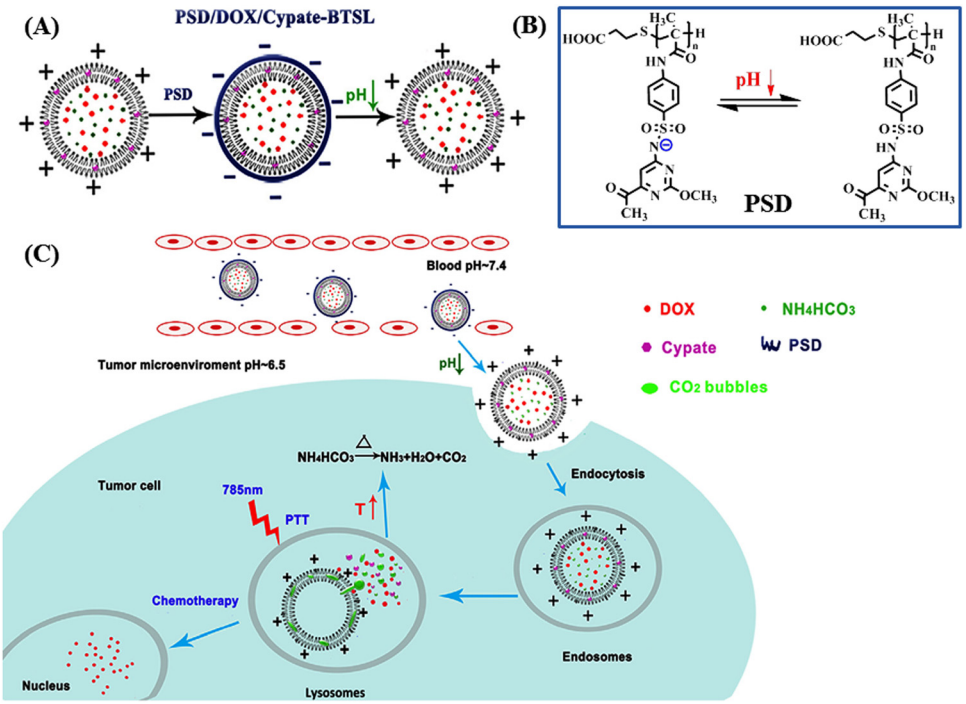

Fig. 8 (A) Schematic presentation of the formation of PSD/DOX/Cypate-BTSL *via* cationic shielding and deshielding. The cationic liposomes are shielded by pH-sensitive PSD to form PSD/DOX/Cypate-BTSL. (B) Different forms of PSD at different pH values. (C) Schematic illustration of NIR-mediated photothermal and chemotherapy of PSD/DOX/Cypate-BTSL. Reproduced with permission from ref. 100 Copyright 2018, Elsevier.

developed material, DPP–BTz/GEM@Lip, was comprised of a conjugated polymer, DPP–BTz, and liposome DSPE–PEG5000–Mal, encapsulating DOX. Upon NIR-II irradiation with a 1064 nm laser (1.0 W cm^{-2}) for 5 min, the thermosensitive liposomes were disrupted, facilitating the release of the anti-cancer drug (GEM) to eradicate tumor cells. This material demonstrated high photothermal conversion efficiency (η) of 51.38% and pH-dependent drug delivery. Zhu and co-workers reported the preparation of the prodrug DCM-S-GEM/PEG compromised of fluorophore dicyanomethylene-4*H*-pyran, which is NIR emissive, connected to the drug molecule gemcitabine *via* a disulfide bond (Fig. 9A).[107] They encapsulated this formation in 1,2-distearoyl-*sn-glycero*-3-phospho-ethanolamine methoxy polyethylene glycol micelles (DSPE-mPEG), providing high water dispersity and tumor-targeting properties. The disulphide bond is cleavable through glutathione, which is much more expressed in tumor cells compared to normal cells. The drug release upon incubation with GSH was monitored by HPLC and mass spectrometry. The disulfide bond was selectively cleaved by glutathione (GSH), cysteine (Cys), and hemocyanin (Hcy) over other amino acids such as Ala, Arg, Asn, Asp, Gln, Glu, Gly, His, Ile, Leu, Phe, Pro, Ser, Thr, Tho, Tyr, and Val which was monitored through fluorescence spectroscopy (Fig. 9B). The authors assessed the cytotoxicity of DCM-S-GEM/PEG in cancerous A549 cells and obtained an IC_{50} value of 0.465 μM, which was very close to the value of 0.443 μM for gemcitabine only. However, DCM-S-GEM/PEG demonstrated stronger fluorescence intensity in cancerous A549 cells owing to the higher concentration of GSH in the cancerous cells as compared to the normal cells QSG-7701 (Fig. 9C). They further employed DCM-S-GEM/PEG for *in vivo* application in xenograft tumors in a mouse model, which provided a longer retention time at the tumor site.

Chen *et al.* developed NIR-responsive ZIF-8/PDA-PEG nanoparticles for chemo-photothermal therapy by encapsulating dual drugs of (−)-epigallocatechin-3-gallate (EGCG) and DOX through self-assembly.[108] This concept also solved the problems regarding the drug co-loading encountered in many MOFs. The drug release behaviour of this nanoformulation was multi responsive, *i.e.*, both pH- and photothermal responsive. Zhang and collaborators addressed the challenges of poor water solubility, premature drug release, rapid systemic clearance, and limited tumor penetration associated with BA (betulinic acid).[109] The prodrug micelles were formulated by combining a poly(ethylene glycol) (PEG)-conjugated BA prodrug (mPEG-SS-BA) and Cypate-conjugated Pluronic triblock copolymer (Pluronic-Cypate). The Pluronic copolymer was equipped with NIR-I-responsive photothermal property through conjugation with the NIR agent Cypate. Under irradiation with an 808-nm laser at 2 W cm^{-2}, F68-Cy exhibited a heating effect with the temperature increasing from 24 °C to 71 °C within 3 min. The NIR-triggered photothermal heating effect of the P-SS-BA/F68-Cy prodrug micelles was found to be concentration and power dependent. In these micelles, BA was linked to the mPEG2K polymer *via* redox-responsive disulfide bonds, which were cleaved to release BA in the presence of a high concentration of GSH in tumor tissues. The combined redox-responsive BA prodrugs and NIR-responsive polymer in the P-SS-BA/F68-Cy

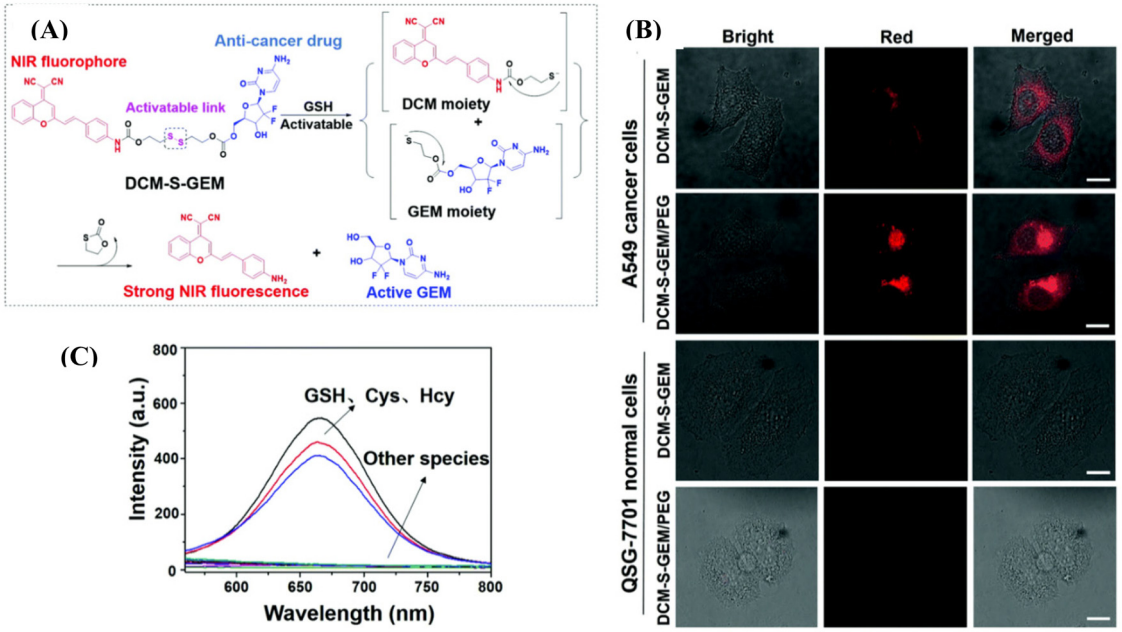

Fig. 9 (A) Response mechanism of DCM-S-GEM with GSH under physiological conditions for drug release, in which the disulfide bond (–S–S–) can be cleaved *via* GSH. (B) Fluorescence images of cancer cells (A549 cells) and normal cells (QSG-7701 cells) with the incubation of DCM-S-GEM and DCM-S-GEM/PEG (10 μM) for 3 h, respectively. Red channels (DCM-NH_2) were obtained by excitation at 485 nm and long-path (630–690 nm) emission filter. (C) Fluorescence spectra toward various amino acids including GSH, Cys, and Hcy (50 μM). All the images share the same scale bar (30 μm). Reproduced with permission from ref. 107 Copyright 2019, the Royal Society of Chemistry.

prodrug micelles resulted in a pronounced synergistic thermo-chemotherapy effect. The photothermal assays demonstrated excellent heating effects under NIR irradiation, with a photothermal conversion efficiency of 29.7%. The *in vitro* cytotoxicity and *in vivo* combined antitumor therapy experiments confirmed the significant synergistic thermo-chemotherapy effect of the P-SS-BA/F68-Cy micelles on tumors. Sun and co-workers reported the development of a dual-function drug delivery system with enhanced antitumor therapy comprised of an NIR-I dye and an anti-angiogenic drug within liposomes (Lip-IR780-Sunitinib) for enhanced antitumor therapy (Fig. 10).[110] The anti-angiogenic drug sunitinib, which targets multiple vascular endothelial growth factor (VEGF) receptors on the tumor endothelial cell surface, and the hydrophobic NIR dye IR780 were loaded in the liposomal matrix. Later, the liposomal bilayer was shown to be disrupted using NIR-I light irradiation for drug release at the tumor site. The IR780-loaded liposomes could destroy the cancer cells by photothermal therapy. The anti-tumor and anti-angiogenic effects aided with photothermal effect originated from the drug and NIR dye-loaded formulation were investigated for *in vitro* and *in vivo* applications.

Lim and colleagues conducted the synthesis of NIR-I-responsive micelles through the addition–fragmentation chain-transfer (RAFT) copolymerization.[111] They synthesized an amphiphilic copolymer comprised of three distinct monomers, *i.e.*, D,L-lactide (LA), *N*-acryloylmorpholine (NAM), and furfuryl methacrylate (FMA). The resulting micelles, formed in an aqueous medium, consisted of a hydrophobic core (PLA) and a hydrophilic shell (PNAM) with a small amount of PFMA. They further induced shell-crosslinking through the Diels–Alder reaction between the furfuryl group of PFMA and the maleimide group of the crosslinker, bis(maleimidoethyl) 3,3′-diselanediyldipropionoate (BMEDSeDP). Simultaneously, the

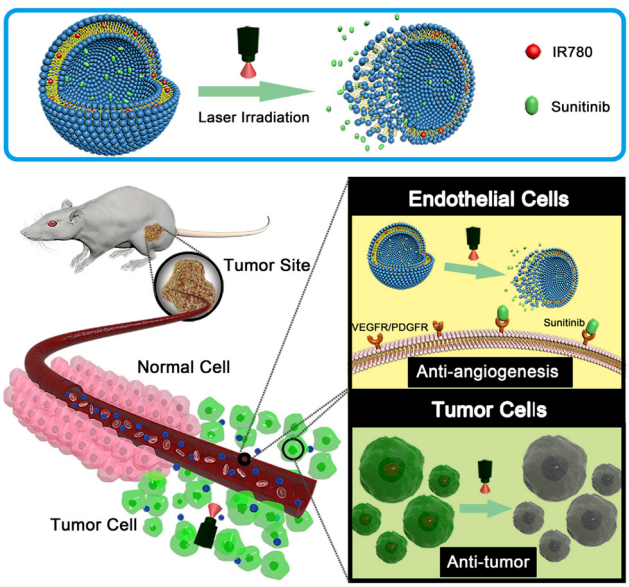

Fig. 10 Schematic design of Lip-IR780-sunitinib-loaded liposomal formulation for photothermal therapy. The photo-triggered release of sunitinib can target VEGF receptors on the cancer cell surface to inhibit tumor angiogenesis. Reproduced with permission from ref. 110 Copyright 2018, Elsevier.

micelles were loaded with both DOX and ICG. The micelles contained advantageous diselenide bonds, acting as crosslinkers, which are known for their easy oxidation under mild stimuli due to their low bond dissociation energy. Upon NIR exposure, the reactive oxygen species (ROS) generated from ICG cleaved the diselenide bonds, disrupting the micellar structure and facilitating the release of DOX. This innovative strategy exploited the responsiveness of diselenide bonds to NIR exposure, providing a controlled and stimulus-responsive mechanism for enhanced therapeutic efficacy. The evaluation of DOX release in HeLa cells revealed notable cytotoxicity upon NIR irradiation. Li *et al.* presented a multifunctional light-activable nanocomplex (MILAN), which was designed for moderate-heat photothermal therapy (PTT) to induce apoptosis without inducing necrosis.[112] This approach helped prevent excessive inflammation in tumors and enhanced cancer immunotherapy against triple-negative breast cancer. This nanocomplex was composed of temperature-sensitive liposomes as carriers, loading indocyanine green (ICG) and glycyrrhetinic acid (GA) in the liposome cavity and phospholipid bilayers, respectively, through lipid film hydration. This strategy improved the co-delivery, successfully encapsulating two types of drugs in the thermosensitive liposomes (Lipo-IG) for NIR-I-responsive release. The entrapment efficiencies of ICG and GA in Lipo-IG were calculated to be approximately 60% and 75%, respectively, at an ICG concentration of around 400 μg mL^{-1}. Both *in vitro* and *in vivo* experiments demonstrated the success of the moderate-heat PTT in inducing apoptosis, enhancing immunotherapy, inhibiting tumors, and eliciting systemic immunity against distant metastatic tumors. Furthermore, this approach established long-term immune memory, effectively preventing tumor recurrence.

Metal-free liposome-based nanoparticles are widely used as nanocarriers for drugs in stimulus-responsive drug delivery but these materials are also associated with drawbacks in biomedical applications such as leakage and fusion of encapsulated drug/molecules, high production cost, and compromised stability given that phospholipids undergo oxidation and hydrolysis-like reaction.[113]

3. NIR-responsive polymeric hydrogels

Thermosensitive hydrogels have emerged as highly promising carriers for targeted drug delivery, offering advantages such as stability, versatile drug loading capacity (ranging from small molecules to large peptides), biocompatibility, and extended release capability.[114,115] Within the category of thermosensitive hydrogels, the PLGA–PEG–PLGA triblock copolymer stands out as one of the most extensively utilized. It facilitates the sustained release of loaded drugs *in vivo* for durations ranging from one week to several months, which is attributed to the gradual degradation of the polyester component.[116,117] Pan *et al.* utilized a collagen-conjugated PLGA polymer-based thermosensitive hydrogel for the NIR-mediated treatment of solid tumors in HER2-positive BT474 tumor-bearing mice.[118] Wang and colleagues developed hybrid nanoparticles based on a combination of a lipid and polymer (LP/ID) for the co-delivery of indocyanine green (ICG) and the anti-cancer drug dichloroacetate (DCA) to achieve a combined photothermal/chemotherapy approach, as shown in the Fig. 11A.[119] The chemical modification of DCA to form an amide bond with PEI resulted in DCA–PEI conjugates, enhancing the loading efficiency and reducing the DCA leakage. The amide bond served as a switch for enzyme-responsive drug release, responding to the overexpressed amidase within tumor cells. Furthermore, the cationic nature of branched PEI allowed it to form complexes with anionic ICG through electrostatic interactions, creating dense hydrophobic electrostatic PEI/ICG complexes. This improved the hydrophobicity of ICG, increasing its entrapment efficiency and reducing its leakage from the hydrophobic cavity. The authors showed efficient cellular uptake of LP/ID by MCF-7 cells, leading to strong cytotoxicity against cancer cells upon NIR-I-irradiation. Both *in vitro* and *in vivo* investigations confirmed the potent anti-cancer effectiveness of this synergistic photothermal/chemotherapy achieved by LP/ID combined with laser treatment. The LP/ICG group exerted more potent cell cytotoxicity than the free ICG after NIR irradiation (as shown in Fig. 11B–D). Alternatively, the *in vivo* study showed that the fluorescence intensity at the tumor sites in the mouse group treated with LP/ID became stronger and was visible up to 24 h than only the ICG-treated mouse, which is a clear indication of the specific distribution of the carrier at the tumor site with a prolonged effect (Fig. 11E).

Sato and co-workers addressed a critical aspect in cancer treatment, *i.e.*, the challenge of tumor-antigen expression heterogeneity. They synthesized a double-conjugated antibody–drug conjugate (ADC) incorporating trastuzumab (Tra) emtansine (T-DM1) and IRDye 700DX NHS ester (IR700), enabling the controlled release of drugs from ADCs through remote activation.[120] Successful Tra and T-DM1 conjugation to IR700 was verified using sodium dodecyl sulfate polyacrylamide gel electrophoresis (SDS-PAGE) and fluorescence imaging (FLI) based on IR700. The NIR-PIT-induced cytotoxicity relied on a photochemical reaction involving silanol ligand release, transforming the hydrophilic conjugates into hydrophobic forms that aggregate. Tra-IR700 and T-DM1-IR700 demonstrated specific binding to HER2-expressing 3T3/HER2 cells (HER2+), and this binding was obstructed by excess Tra or T-DM1, respectively, affirming their HER2 specificity. Neither Tra-IR700 nor T-DM1-IR700 exhibited binding to HER2-negative MDAMB-468 cells. TDM1-IR700 exhibited specific toxicity toward HER2-expressing cells, and S-Me-DM1 induced cytotoxicity in various cancer cell lines at an appropriate concentration. The effects of NIR-PIT on 3T3/HER2 cells bound by Tra-IR700 or T-DM1-IR700 were confirmed through microscopic observations before and immediately after NIR-light irradiation. After NIR light exposure (4 J cm^{-2}), HER2+ 3T3/HER2 cells displayed necrosis *via* propidium iodide (PI) staining, while the HER2− MDAMB-468-luc-GFP cells remained unaffected. Co-culturing HER2− and HER2+ cells demonstrated that NIR-PIT with Tra-IR700 or

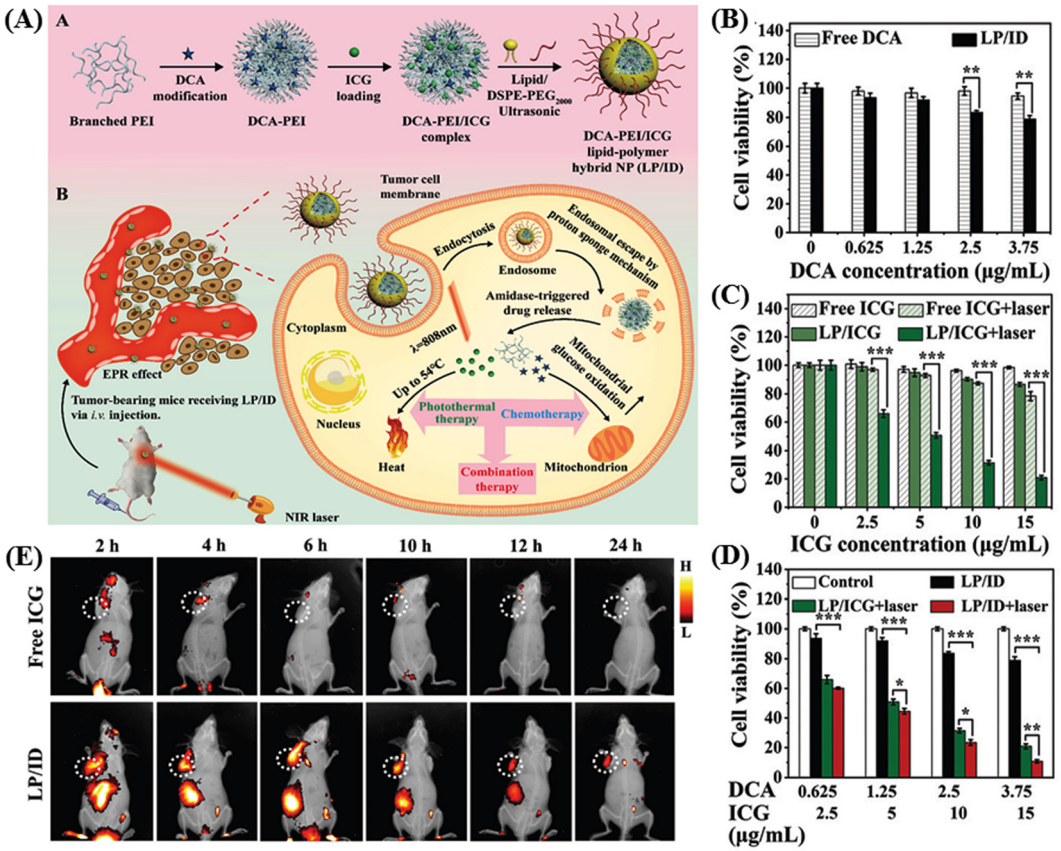

Fig. 11 Schematic graph illustrating the construction of LP/ID and its synergistic anti-cancer mechanism mediated by PTT and chemotherapy (A). *In vitro* therapeutic efficacy analysis. Cell viabilities of MCF-7 cells subjected to (B) single chemotherapy, (C) single PTT and (D) combination of PTT and chemotherapy for 24 h with or without laser irradiation. Data are shown as mean ± S.D. (n = 3). *P < 0.05, **P < 0.01 and ***P < 0.001. *In vivo* NIRF imaging of MCF-7 tumor-bearing nude mice after IV injection (E). Reproduced with permission from ref. 119 Copyright 2022, the Royal Society of Chemistry.

T-DM1-IR700 specifically induced necrosis in mixed *in vitro* cultures. This technology was investigated in a mixed tumor model comprised of HER2+ 3T3/HER2 and HER2-MDAMB-468-luc-GFP cells. This system demonstrated NIR-light-triggered drug release in heterogeneous tumors, leading to the effective eradication of tumor cells. Li and colleagues developed a facile approach to prepare an injectable hydrogel (KPFe) using an anticancer peptide (KLLKLLKKL LKLLK-NH_2), protocatechualdehyde (PCA) and Fe^{3+} ions *via* dynamic bond formation for localized delivery for cancer treatment (Fig. 12).[121] The dynamic imine linkages and strong Fe(III)–catechol coordination interactions provided a supramolecular hydrogel. This material has good self-healing properties, mechanical stability, and thermal and pH responsiveness. The inherent NIR absorption properties of this hydrogel originating from the Fe(III)–catechol coordination are crucial for photothermal therapy. The KPFe hydrogel could also encapsulate the chemotherapeutic drug DOX (KPFD) through multiple physical interactions. The acidic tumor microenvironment and hyperthermia effects resulting from the NIR trigger enabled the on-demand release of DOX. The KPFD hydrogel could perform dual chemo-photodynamic therapy against liver cancer with minimal side effects.

4. NIR-responsive supramolecular vesicles

The development of multifunctional therapeutic systems that integrate spatiotemporally controlled delivery, multimodal synergistic therapy, and prolonged retention at affected sites of disease is paramount. Researchers are increasingly evaluating supramolecular vesicles for the creation of smart drug delivery systems due to their unique ability to encapsulate drugs within their cavities and facilitate controlled release.[122,123] These vesicles offer advantages in delivering drugs to specific pathological sites with microenvironmental changes. Alternatively, hydrogel-based drug delivery systems have the ability to provide localized and sustained release of therapeutic agents in pathological tissues, minimizing their side effects and increasing their bioavailability. However, traditional hydrogels are associated with limitations such as non-responsiveness to surrounding conditions, uncontrollable release, and lack of multifunctionality. Thus, to address these issues, researchers are focusing on developing stimulus-responsive and injectable multifunctional hydrogels for precise and personalized cancer treatment. Specifically, near-infrared

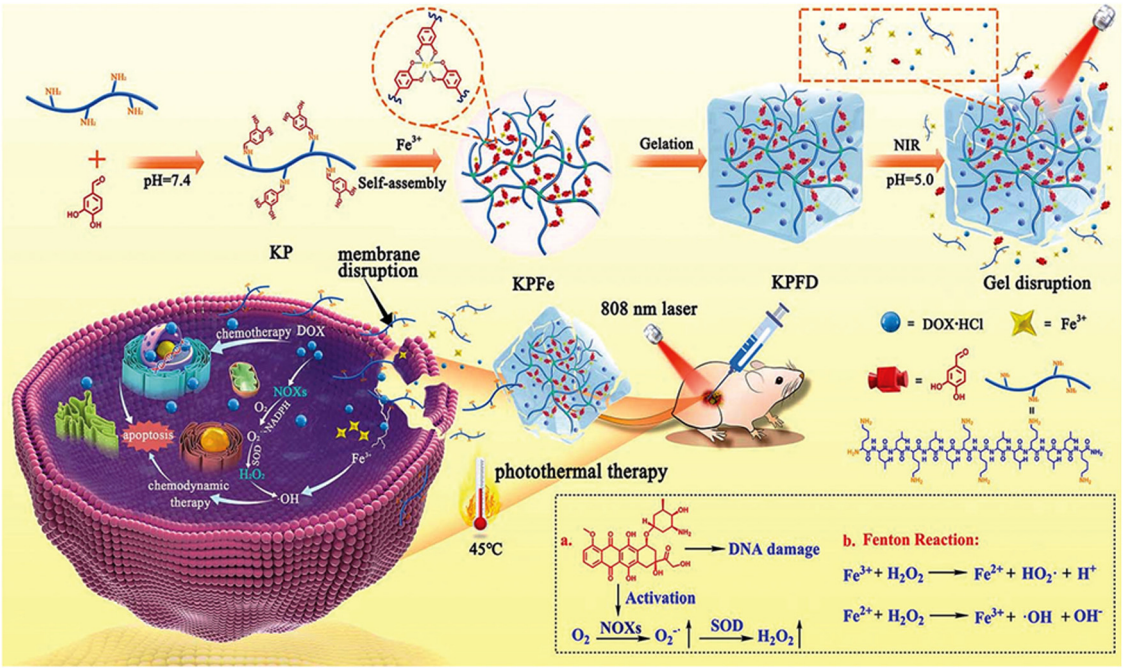

Fig. 12 Illustration of the self-assembly process of the anticancer peptide of KL, PCA and Fe^{3+} ions for the preparation of an injectable hydrogel and its application in synergistic photothermal–chemotherapy. Reproduced with permission from ref. 121 Copyright 2022, the Royal Society of Chemistry.

(NIR)-triggered thermal-responsive hydrogels are gaining attention due to their deep-tissue penetration capacity and spatio-temporally controllable drug release. This part of the review explores the effectiveness of these systems in the context of drug delivery.

Wang *et al.* developed supramolecular vesicles with the combination of NIR-absorbing perylene diimide dye G and water soluble pillar[5]arene for chemo-photothermal tumor therapy.[124] These supramolecular vesicles exhibited chemotherapeutic potential *via* the rapid release of DOX under acidic conditions. Moreover, an excellent photothermal conversion performance was obtained from these vesicles under a 730 nm NIR-I laser given that the temperature of the vesicles rapidly increased to 62.4 °C within 10 min of irradiation.

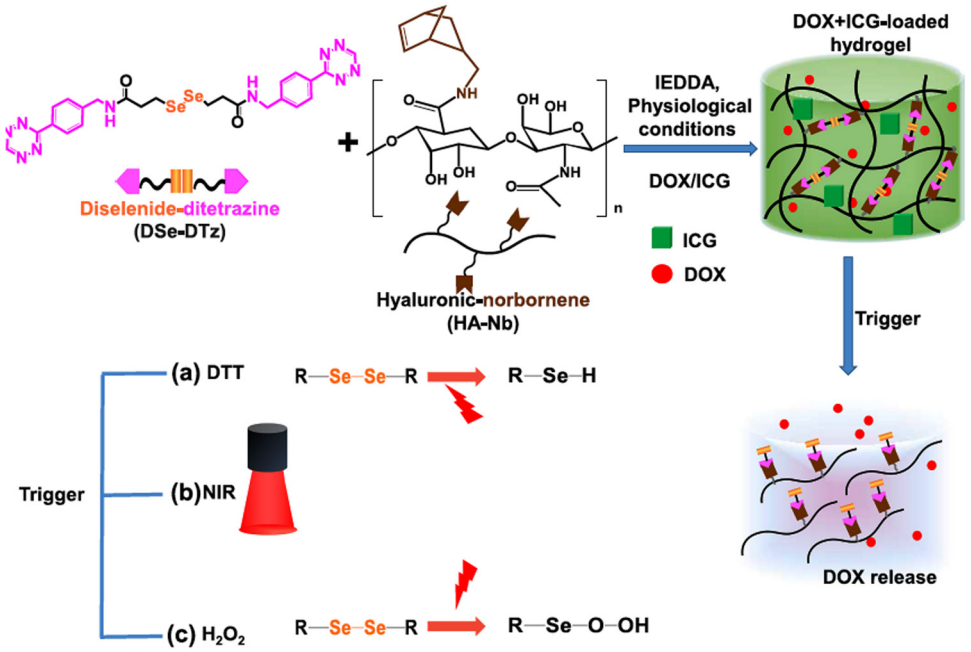

Scheme 3 Schematic presentation of the synthesis of multi-responsive hyaluronic acid-derived hydrogels and mechanism of cleavage of diselenide bonds under various triggers and drug release. Reproduced with permission from ref. 125 Copyright 2022, Elsevier.

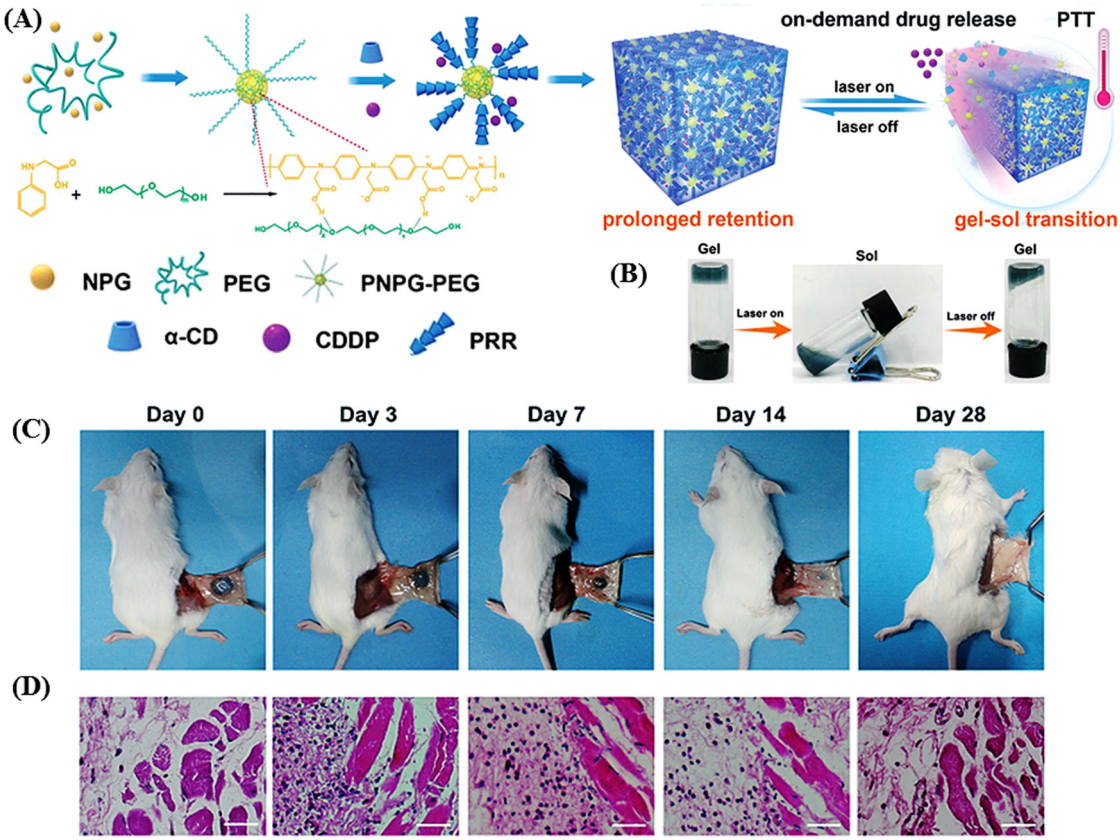

Fig. 13 Schematic illustration of the fabrication of the NIR-II light-responsive hydrogel based on supramolecular self-assembly and its application in NIR-triggered cisplatin release and repeated chemophotothermal therapy. (B) Thermo-sensitive and reversible gel–sol transition of the hydrogel under 1064 nm laser irradiation. (C) Photographs of the subcutaneously injected hydrogels at different intervals post injection and (D) H&E staining of the corresponding subcutaneous tissues surrounding the hydrogel (the nuclei were stained bluish violet, and the cytoplasm and extracellular matrix were stained pink. Scale bar: 40 μm). Reproduced with permission from ref. 126 Copyright 2019, the Royal Society of Chemistry.

Jo *et al.* reported the preparation of NIR-light responsive hyaluronic acid-based hydrogels by applying bio-orthogonal click chemistry (Scheme 3).[125] They utilized a diselenide-based cross-linker with two terminal ditetrazine groups and combined it with norbornene-functionalized hyaluronic acid to form a porous hydrogel. The anticancer drug DOX and NIR-active dye indocyanine green (ICG) were encapsulated within the hydrogel, where ICG was capable of producing reactive oxygen species (ROS) by absorbing NIR-I light. The ROS further facilitated the cleavage of diselenide bonds and release of DOX within the tumor cells. Their synthesized hydrogel also exhibited environment-responsive drug release behaviour, *i.e.*, reducing environment [10 mmol of 1,4-dithiothreitol (DTT)], enhanced the speed of DOX release, whereas oxidizing (0.5% H_2O_2) environment facilitated sustained release in breast cancer cells (BT-29).

Ruan *et al.* developed an injectable, NIR-II light-activated thermosensitive hydrogel with supramolecular self-assembly of a conjugated poly(*N*-phenylglycine) polymer and α-CD for the photothermal treatment of triple-negative breast cancer, as schematically shown in Fig. 13A.[126] In this hydrogel, the conjugated polymer poly(*N*-phenylglycine) not only served as a building block together with the poly(ethylene glycol) chains but also provided NIR-responsive and thermosensitive properties for photothermal conversion. Upon NIR laser irradiation at 808 nm and 1064 nm, the conjugated polymer exhibited high photothermal conversion efficiency of 40% and 41%, respectively. Both the *in vitro* and *in vivo* studies showed that under NIR-II (1064 nm) laser, this hydrogel was capable of NIR-triggered on-demand sustained release of cisplatin in cancer cells through a thermo-responsive gel–sol transition (Fig. 13B). The *in vivo* stability of the hydrogel was also accessed by this group, and it was observed that the hydrogel kept its integrity for up to 7 days, whereas its overall size gradually decreased. After 28 days post-injection, together with the complete degradation of the hydrogel, inflammation was also cured, as evident from the haematoxylin and eosin (H&E) staining (as shown in Fig. 13C and D).

Liu *et al.* demonstrated an injectable NIR-activated three-dimensional hydrogel with the supramolecular assembly of a conjugated polymer [poly(*N*-phenylglycine)] and α-CD for the sustained and on-demand release of the anticancer agent DOX in tumor-bearing mice.[127] The conjugated-polymer facilitated the photothermal activity by converting light into heat, whereas α-CD supported the backbones by crosslinking each other to form a network-like structure. Their designed

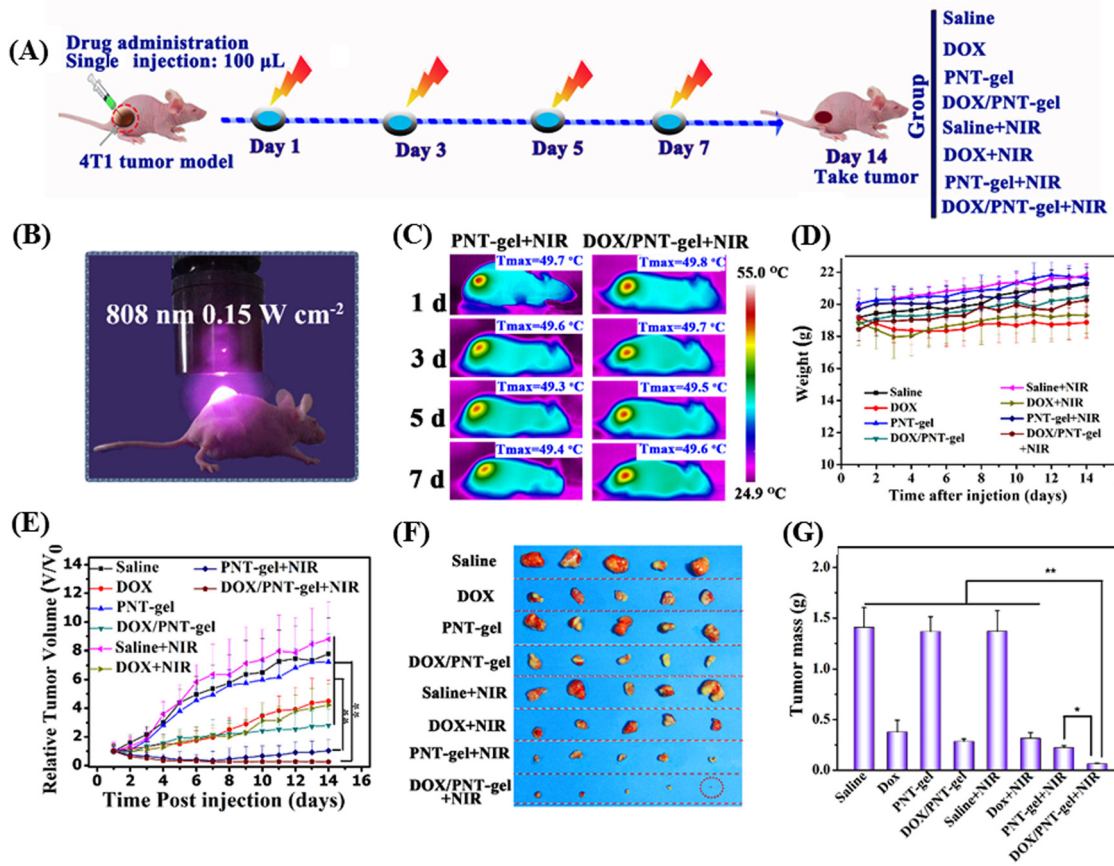

Fig. 14 *In vivo*-repeated PTT and chemotherapy-mediated by PNT-gels. (A) Schematic diagram of the therapeutic procedure. (B) Digital photograph of mice treated by 808 nm NIR laser. (C) Infrared thermal images of mice taken at the maximum steady temperatures during each treatment (808 nm laser; irradiation time: 5 min; power: 0.15 W cm^{-2}). (D) Body weight changes in 4T1 tumor-bearing mice upon various treatments. (E) Relative tumor volume changes over the treatment period. (F) Resected tumors obtained after 14 days of treatment and (G) the corresponding tumor weights of different treatment groups. Reproduced with permission from ref. 127 Copyright 2019, Elsevier.

polymer backbones exhibited a photothermal conversion efficiency of 52.6%. Under 808 nm laser irradiation, the photoresponsive linkers in the hydrogel could convert the light energy in the local hyperthermia environment of the tumor cells, where the maximum temperature reached up to 50 °C. Alternatively, this polymeric hydrogel also showed photothermally-triggered gel–sol conversion and sustained release of DOX in 4T1 tumor-bearing mice. Photothermal chemotherapy was given to tumor-bearing mice (treated and control) under 808 nm NIR laser irradiation (ultralow-dose of 0.15 W cm^{-2}) up to 14 days, as shown in Fig. 14A and B. The temperature in the tumor site of the mouse group treated with PNT-gel and DOX/PNT-gel increased rapidly, and finally reached 49.5 °C and 49.9 °C, respectively (Fig. 14C). The tumor volumes of the DOX/PNT-gel + NIR group mice were subsequently quenched after NIR irradiation (as shown in Fig. 14D and E).

We present a summary of the NIR-responsive materials according to their features, photothermal properties, and biological applications in Table 1. For the ease of comparison, the temperature changes are indicated as (T-37) °C, where 37 °C represents the standard biological temperature.

5. Conclusions and future perspectives

NIR light is a magical tool in the biomedical engineering field for both bio-imaging purposes and photothermal chemotherapy given that it can deeply penetrate biological tissues with minimum interference. In this review, we summarized the recent advances in the design, preparation and applications of NIR-responsive smart carriers from different realms of materials. Most of the systems exhibit multi-responsive theranostic applications, *i.e.*, pH-dependent drug release, cellular receptor-specific delivery of chemotherapeutics, heat-mediated drug release, and photothermal tumor damage. Carbon-based nanomaterials can be promising tools for researchers in the development of NIR-activated drug delivery given that they exist in different forms of allotropes together with diverse properties. Furthermore, the photoconversion efficiencies of these carbon-based nanoparticles can be enhanced by modifying their surface with biocompatible polymers.[131] In the case of gold-based nanoparticles, their size can be modulated for triggering their NIR-absorbing capabilities. Moreover, gold-based nanoparticles offer a wide opportunity for different functionalities to

Table 1 Brief summary of the properties and applications of NIR-responsive materials discussed in this review (PTA: photothermal agent, Ex: excitation, PCE: photothermal conversion efficiency, NA: not applicable, Max.: maximum, ΔT: temperature increase from 37 °C, and Ref.: references)

Category	Name	PTA	NIR Ex (nm)	PCE (%)	Max. laser power (W cm^{-2})	Application	ΔT (T-37) °C	Ref.
Carbon-based nanomaterial	MWCNTs–TAM–LEN	MWCNTs	808 (NIR-I)	NA	2.0	MCF-7 cells	22.0	32
	DNA-SWCNTs-liposome	SWCNTs	1122 (NIR-II)	NA	0.8	RAW 264.7 macrophages	12.0	33
	GO–PEG–Fol/Dox	GO	810 (NIR-I)	NA	1.4	HDFa, MCF7 and MDA-MB-231 cells	7.5	42
	AuNRs/GO@PDA	AuNR-GO	808 (NIR-I)	36.1%	2.0	MCF-7 cells	NA	39
	ICG/DOX/GO-PPF68	GO	808 (NIR-I)	NA	2.0	MCF-7/ADR tumor cells and tumor-bearing mice	14.0	45
	F127-GO-DOX	GO	808 (NIR-I)	NA	0.5	A549 cells and tumor-bearing mice	NA	46
	PTX@HCNs	HCNs	808 (NIR-I)	NA	3.0	HCT 116 cells	19.0	49
	NIR-II-CQDs/DOX/BP	CQDs	808 (NIR-I) and 1064 (NIR-II)	77.3% and 61.4%	0.6	HeLa cells and 4T1 tumor-bearing mice	18.7	52
	M/A-CQDs@CpG	CQDs	808 (NIR-I)	37.7%	2.0	4T1 mouse breast cancer cell line and tumor-bearing mice	18.0	53
	CQD@Co_3O_4	CQDs	1064 (NIR-I)	51.1%	0.6	HeLa cells and tumor-bearing mice	21.8	54
	PDA-PEI@N,S-CQDs/Dox	CQDs	808 (NIR-I)	30%	2.0	HeLa cells	NA	55
	RHNS-cyclodextrin-PGEA	RHNS	1064 (NIR-II)	59.2%	0.5	4T1 and HEK293 cell lines and breast cancer-bearing Balb/c nude mice	23.0	56
Metal nanoparticles	F127-NO-GEL-AuNS-DMXXA	AuNSs	808 (NIR-I)	NA	2.0	4T1 cells and tumor-bearing mice	13.0	72
	Au NR@Curcumin	AuNRs	808 (NIR-I)	NA	0.9	A549, KB and HepG2 cells and tumor-bearing mice	14.2	13
	CS/HPC/GP-Fe_3O_4@PDA	Fe_3O_4	808 (NIR-I)	48.9%	2.0	A549 and HeLa cells	3.0	128
	AuNS-Wed-Lip	AuNSs	808 (NIR-I)	NA	2.0	143B tumor cells and S180 tumor-bearing mice	6.0	75
	AuSi@FePB	AuNSs	1064 (NIR-II)	38.8%	1.0	4T1 cells and tumor-bearing mice	17.3	76
	AuHNR@MnO_2@CS	AuHNRs	1064 (NIR-II)	33.2%	0.69	MB49 cells and tumor-bearing mice	5.6	77
	RGD/DOX–pAS@AuNC	AuNCs	808 (NIR-I)	85.5%	0.5	HeLa cells and tumor-bearing mice	20.0	83
	HAuNS@PEG-bio	HAuNS	1064 (NIR-II)	63%	1.5	4T1 cells and tumor-bearing mice	13.2	84
	^{131}I-AuNFs	AuNFs	1064 (NIR-II)	NA	1.0	4T1 cells and tumor bearing mice	23.4	85
	AuNPs-DBCO-RGD and AuNPs-DBCO-RGD	AuNPs	808 (NIR-I)	53.7%	1.25	Murine embryonic3T3 cells, 4T1 cells, and tumor-bearing mice	NA	86
	dpGCS NCs	Au@Cu_{2-x}Se core–shell nanocrystals	1064 (NIR-II) and 808 (NIR-I)	71.0%	1.5	U87-MG cells and tumor-bearing mice	33.3	88
Metal free nanomaterial	FA-PEG@BPQD@DOX	BPQDs	808 (NIR-I)	NA	2.0	293T cells and tumor-bearing mice	19.2	96
	BP@DOX/PEG-FA	BPNSs	808 (NIR-I)	38%	0.85	B16F10 cells and tumor bearing mice	19.7	97
	T-DPPT/PTX/PCL-PEEP	T-DPPT	808 (NIR-I)	70%	1.0	4T1 cells and tumor-bearing mice	20.0	98
	Lip-IR780-Sunitinib	IR780	808 (NIR-I)	NA	1.0	4T1 cells and tumor-bearing mice	43.0	110
	PSD/DOX/Cypate-BTSL	Cypate	785 (NIR-I)	NA	1.6	4T1 cells and tumor-bearing mice	5.0	100
	PLDT/PLDD/DMXAA	DTTP	808 (NIR-I)	NA	1.0	LLC cells and tumor-bearing mice	23.3	101
	PATSL	TB1 dye	808 (NIR-I)	68.8%	0.8	U87 glioma cells and mice bearing sub-cutaneous glioma	12.9	102
	EGCG@ZIF-PDA-PEG-DOX	ZIF-8	808 (NIR-I)	NA	2.0	HeLa cells and tumor-bearing mice	31.4	108
	P-SS-BA/F68-Cy	Cypate	808 (NIR-I)	29.7%	2.0	4T1 cell line and tumor-bearing mice	34.0	19
	Lipo-ICG/HA-CpG,	ICG	808 (NIR-I)	NA	2.0	4T1 cell line and tumor-bearing mice	6.0	113
Polymeric hydrogel	DCA-PEI/ICG lipid-polymer hybrid NP (LP/ID)	ICG	808 (NIR-I)	NA	1.0	MCF-7 cells and tumor-bearing mice	25.6	119
	KPFe hydrogels	Fe(III)–catechol complex	808 (NIR-I)	24.7%	2.0	HepG2 cells and tumor-bearing mice	11.6	121
	DOX-ICG loaded hydrogel	ICG	808 (NIR-I)	NA	4.0	HEK-293 and BT-20 cells	12.0	125
	DPP-BTz/GEM@Lip	DPP-BTz	1064 (NIR-II)	51.38%	1.0	NIH-3T3, HeLa, and PANC-1 cells and PANC-1 tumor-bearing mice	25.4	106

Table 1 (*continued*)

Category	Name	PTA	NIR Ex (nm)	PCE (%)	Max. laser power (W cm^{-2})	Application	ΔT (T-37) °C	Ref.
Supramolecular vesicles	PDI/WP5/Dox	PDI	730 (NIR-I)	44.5%	1.5	MCF7 cells	25.4	124
	PNPG–PEG/α-CD hydrogel	Poly(*N*-phenylglycine)	808 (NIR-I) 1064 (NIR-II)	40% and 41%	0.5	MDA-MB-231 cells and tumor-bearing mice	15.3 and 16.9	127
	PPG-peg/α-CD/Dox	Poly(*N*-phenylglycine)	808 (NIR-I)	52.6%	0.3	4T1 cells and tumor-bearing mice	13.0	127
	CPT@DOX-UCST/PPy	PPy	808 (NIR-I)	26.2%	1.0	4T1 cells and tumor-bearing mice	9.9	129
	WP5/TANI	WP5	808 (NIR-I) and 1064 (NIR-II)	11.9% and 32.0%	3.0	L02 and CT26 cells and CT26 tumor-bearing mice	5.0	130

be attached to their surface through both covalent and non-covalent interactions. Between them, covalent attachment of the drugs to gold nanoparticles is preferable to overcome challenges such as poor drug loading and delayed drug release. Some of the added advantages of nanomicelles and polymeric hydrogels are their tailor-made structural design, stability, and biocompatibility. Therefore, these materials are mostly explored as drug carriers in the field of biomedical engineering. Moreover, they are being functionalized with photothermal agents for utilization as light-activated targeted drug carriers. The recently reported supramolecular crosslinked polymers with NIR-activable thermosensitive system were depicted as a fascinating approach for the sustained release of chemotherapeutics *via* adjustable gel–sol phase transition.[132–134]

Despite the tremendous efforts in this emerging field of NIR-responsive drug delivery, there are still some drawbacks that need to be properly addressed for the sake of therapeutic efficacy and safety. Although NIR-II light (with 1064 nm wavelength) can deeply penetrate tissue compared to visible or UV light, it is not more than several centimetres.[135] Moreover, most of the scientific studies on NIR-responsive materials have been done with the small animal, *e.g.*, rodents, but curing of tumors, which are surrounded by thick layers of tissues or muscles, in large animal model or human beings is difficult with these NIR-responsive technologies. In addition, the application of NIR-II light with high power density and stronger penetration efficiency may result in normal tissue damage.[136] Modifications in the design of carriers is an another factor, where improvements are needed. The major disadvantages of carbon-based stimulus-responsive nanomaterials are their high toxicity and unwanted accumulation within cells and tissues. Moreover, the poor drug loading efficacy and formation of stable nanocomposites are other issues associated with carbon-based nanomaterials in the case of non-covalent conjugation with the drugs molecules. Although the biocompatibility issue has been overcome by employing stimulus-responsive polymer and micellar systems, to achieve photothermal chemotherapy, some NIR active materials must be embedded within these systems.[137] Therefore, direct exposure of the photothermal agents to NIR irradiation is difficult, thus leading to an inferior photothermal conversion effect.[138] NIR-responsive supramolecular assemblies also face challenges such as uncontrolled release of drugs and leakage of photothermal nanoagents, leading to a limited treatment effect.[139]

Furthermore, the development of multi-responsive drug carriers often leads to complexity in the systems, which will decrease their reproducibility and industrial value. Therefore, to meet the biomedical demand in cancer therapy, reliable, biocompatible and multi-responsive "smart" materials must be produced, where controlled and on-demand drug release will be prioritized.

Author contributions

All authors enthusiastically participated in writing this manuscript.

Conflicts of interest

The authors declare no conflict of interest.

Acknowledgements

We wish to acknowledge all researchers working on NIR-responsive materials for their passion and hard work for the development of impressive contribution. AK would like to thank CCRAS for the postdoctoral fellowship. AS acknowledge CSIR for his doctoral fellowship. We acknowledge the financial and infrastructural support from IISER Bhopal.

References

1 H. K. Matthews, C. Bertoli and R. A. de Bruin, *Nat. Rev. Mol. Cell Biol.*, 2022, **23**, 74–88.
2 J. Ferlay, M. Colombet, I. Soerjomataram, D. M. Parkin, M. Piñeros, A. Znaor and F. Bray, *Int. J. Cancer*, 2021, **149**, 778–789.
3 R. L. Siegel, A. N. Giaquinto and A. Jemal, *CA-Cancer J. Clin.*, 2024, **74**, 12–49.
4 U. Hani, S. Wahab, A. Siddiqua, R. A. M. Osmani and M. Rahmathulla, *J. Pharma. Innov.*, 2021, 1–24.
5 A. Tiwari, S. Saraf, A. Jain, P. K. Panda, A. Verma and S. K. Jain, *Drug Delivery Transl. Res.*, 2020, **10**, 319–338.
6 K. Bukowski, M. Kciuk and R. Kontek, *Int. J. Mol. Sci.*, 2020, **21**, 3233.
7 M. Nikolaou, A. Pavlopoulou, A. G. Georgakilas and E. Kyrodimos, *Clin. Exp. Metastasis*, 2018, **35**, 309–318.
8 M. A. Younis, H. M. Tawfeek, A. A. Abdellatif, J. A. Abdel-Aleem and H. Harashima, *Adv. Drug Delivery Rev.*, 2022, **181**, 114083.
9 A. Tewabe, A. Abate, M. Tamrie, A. Seyfu and E. Abdela Siraj, *J. Multidiscip. Healthcare*, 2021, 1711–1724.
10 J. Wang, X. Wu, P. Shen, J. Wang, Y. Shen, Y. Shen, T. J. Webster and J. Deng, *Int. J. Nanomed.*, 2020, 1903–1914.
11 C. Xu and K. Pu, *Chem. Soc. Rev.*, 2021, **50**, 1111–1137.
12 M. Zhang, W. Hu, C. Cai, Y. Wu, J. Li and S. Dong, *Mater. Today Bio*, 2022, **14**, 100223.
13 Y. Zhou, H. Ye, Y. Chen, R. Zhu and L. Yin, *Biomacromolecules*, 2018, **19**, 1840–1857.
14 F. Li, Y. Qin, J. Lee, H. Liao, N. Wang, T. P. Davis, R. Qiao and D. Ling, *J. Controlled Release*, 2020, **322**, 566–592.
15 Y. Tang and G. Wang, *J. Photochem. Photobiol., C*, 2021, **47**, 100420.
16 C. Kong and X. Chen, *Int. J. Nanomed.*, 2022, **17**, 6427.
17 R. Vankayala and K. C. Hwang, *Adv. Mater.*, 2018, **30**, 1706320.
18 Y. Zhang, S. Zhang, Z. Zhang, L. Ji, J. Zhang, Q. Wang, T. Guo, S. Ni, R. Cai and X. Mu, *Front. Chem.*, 2021, **9**, 728066.
19 D. An, J. Fu, B. Zhang, N. Xie, G. Nie, H. Ågren, M. Qiu and H. Zhang, *Adv. Funct. Mater.*, 2021, **31**, 2101625.
20 K. D. Patel, R. K. Singh and H.-W. Kim, *Mater. Horiz.*, 2019, **6**, 434–469.
21 J. Saleem, L. Wang and C. Chen, *Adv. Healthcare Mater.*, 2018, **7**, 1800525.
22 S. Zheng, Y. Tian, J. Ouyang, Y. Shen, X. Wang and J. Luan, *Front. Chem.*, 2022, **10**, 990362.
23 N. Dubey, S. Dhiman and A. L. Koner, *ACS Appl. Nano Mater.*, 2023, **6**, 4078–4096.
24 D. Sahoo, T. Mitra, K. Chakraborty and P. Sarkar, *Mater. Today Chem.*, 2022, **25**, 100987.
25 X. Bao, Y. Yuan, J. Chen, B. Zhang, D. Li, D. Zhou, P. Jing, G. Xu, Y. Wang and K. Holá, *Light: Sci. Appl.*, 2018, **7**, 91.
26 C. Zhao, J. Kang, Y. Li, Y. Wang, X. Tang and Z. Jiang, *Cyborg. Bionic Syst.*, 2023, **4**, 0022.
27 Z. Li, A. L. B. de Barros, D. C. F. Soares, S. N. Moss and L. Alisaraie, *Int. J. Pharm.*, 2017, **524**, 41–54.
28 D. Lu, R. Tao and Z. Wang, *Front. Chem. Sci. Eng.*, 2019, **13**, 310–323.
29 S. M. Hosseini, J. Mohammadnejad, R. Najafi-Taher, Z. B. Zadeh, M. Tanhaei and S. Ramakrishna, *ACS Appl. Bio Mater.*, 2023, **6**, 1323–1338.
30 D. Pantarotto, J.-P. Briand, M. Prato and A. Bianco, *Chem. Commun.*, 2004, 16–17.
31 N. Panwar, A. M. Soehartono, K. K. Chan, S. Zeng, G. Xu, J. Qu, P. Coquet, K.-T. Yong and X. Chen, *Chem. Rev.*, 2019, **119**, 9559–9656.
32 W. Yi, P. Zhang, J. Hou, W. Chen, L. Bai, S. Yoo, A. Khalid and X. Hou, *Int. J. Biol. Macromol.*, 2018, **120**, 1525–1532.
33 S. Z. M. Madani, M. M. Safaee, M. Gravely, C. Silva, S. Kennedy, G. D. Bothun and D. Roxbury, *ACS Appl. Nano Mater.*, 2020, **4**, 331–342.
34 E. Demirel and Y. Y. Durmaz, *Eur. Poly. J.*, 2023, **186**, 111841.
35 S. Parvaneh, M. Pourmadadi, M. Abdouss, S. A. Pourmousavi, F. Yazdian, A. Rahdar and A. M. Díez-Pascual, *Int. J. Biol. Macromol.*, 2023, **241**, 124566.
36 K. Ma, W. Li, G. Zhu, H. Chi, Y. Yin, Y. Li, Y. Zong, Z. Guo, L. Wang and W. Xu, *J. Drug Target.*, 2021, **29**, 884–891.
37 F. Islam, F. A. Khan, N. M. Khan, S. Ahmad, A. A. Alsaiari, M. Almehmadi, N. Ahmad, Z. Ul-Haq, A. K. Jan and M. Allahyani, *ACS Omega*, 2023, **8**(23), 20550–20560.
38 Y. Wang, J. Hu, D. Xiang, X. Peng, Q. You, Y. Mao, D. Hua and J. Yin, *Colloids Surf.*, 2020, **596**, 124711.
39 Z. Qi, J. Shi, B. Zhu, J. Li and S. Cao, *J. Mater. Sci.*, 2020, **55**, 14530–14543.
40 M. Ramezani Farani, P. Khadiv-Parsi, G. H. Riazi, M. Shafiee Ardestani and H. Saligheh Rad, *Appl. Nanosci.*, 2020, **10**, 1205–1217.
41 M. Georgieva, Z. Gospodinova, M. Keremidarska-Markova, T. Kamenska, G. Gencheva and N. Krasteva, *Pharmaceutics*, 2021, **13**, 424.
42 N. Mauro, C. Scialabba, S. Agnello, G. Cavallaro and G. Giammona, *Mater. Sci. Eng., C*, 2020, **107**, 110201.
43 Z. Peng, Q. Chang, M. Xing and F. Lu, *Int. J. Nanomed.*, 2023, 971–986.
44 Y. Chen, Y. He, X. Wang, F. Lu and J. Gao, *Oncol. Rep.*, 2019, **41**, 2126–2136.

45 M. Wang, J. Wu, Y. Li, F. Li, X. Hu, G. Wang, M. Han, D. Ling and J. Gao, *J. Controlled Release*, 2018, **288**, 34–44.
46 B. Li, L. Zhang, Z. Zhang, R. Gao, H. Li, Z. Dong, Q. Wang, Q. Zhou and Y. Wang, *RSC Adv.*, 2018, **8**, 1693–1699.
47 W. Zhang, J. Dai, G. Zhang, Y. Zhang, S. Li and D. Nie, *Nanoscale Res. Lett.*, 2018, **13**, 1–10.
48 S. D. Dutta, K. Ganguly, J. Hexiu, A. Randhawa, M. Moniruzzaman and K. T. Lim, *Macromol. Biosci.*, 2023, 2300096.
49 X. Wang, Y. Liu, Z. Liu, J. Hu, H. Guo and F. Wang, *Biochem. Biophys. Res. Commun.*, 2018, **495**, 867–872.
50 D. F. Báez, *Pharmaceutics*, 2023, **15**, 2286.
51 H. Wang, G. Cao, Z. Gai, K. Hong, P. Banerjee and S. Zhou, *Nanoscale*, 2015, **7**, 7885–7895.
52 B. Geng, W. Shen, P. Li, F. Fang, H. Qin, X. K. Li, D. Pan and L. Shen, *ACS Appl. Mater. Interfaces*, 2019, **11**, 44949–44960.
53 S. Liu, M. Zhang, H. Yu, X. Sun, Q. Li, M. Yang, X. Qiu, H. Su, A. Gong and F. Du, *ACS Appl. Mater. Interfaces*, 2023, **15**, 7700–7712.
54 N. Wang, T. Dong, W. Shi, L.-A. Li, M.-X. Ye, X.-Y. Fu, Z.-F. Yan and Y.-G. Meng, *J. Mater. Chem. B*, 2023, **11**, 6372–6382.
55 Q. Shu, J. Liu, Q. Chang, C. Liu, H. Wang, Y. Xie and X. Deng, *ACS Biomater. Sci. Eng.*, 2021, **7**, 5497–5505.
56 N. Zhao, W. Fan, X. Zhao, Y. Liu, Y. Hu, F. Duan and F.-J. Xu, *ACS Appl. Mater. Interfaces*, 2020, **12**, 11341–11352.
57 Z. Zhang, L. Wang, J. Wang, X. Jiang, X. Li, Z. Hu, Y. Ji, X. Wu and C. Chen, *Adv. Mater.*, 2012, **24**, 1418–1423.
58 Z. Peng, X. Liu, W. Zhang, Z. Zeng, Z. Liu, C. Zhang, Y. Liu, B. Shao, Q. Liang and W. Tang, *Environ. Int.*, 2020, **134**, 105298.
59 W. Liu and G. Speranza, *C*, 2019, **5**, 72.
60 J. B. Vines, J.-H. Yoon, N.-E. Ryu, D.-J. Lim and H. Park, *Front. Chem.*, 2019, **7**, 167.
61 Y. Zhang, S. Hao, J. Zuo, H. Guo, M. Liu, H. Zhu and H. Sun, *ACS Biomater. Sci. Eng.*, 2022, **9**, 340–351.
62 T. Wang, K. Niu, S. Ni, W. Zhang, Z. Liu and X. Zhang, *ACS Sustainable Chem. Eng.*, 2022, **10**, 1585–1594.
63 J. F. Hainfeld, M. J. O'Connor, P. Lin, L. Qian, D. N. Slatkin and H. M. Smilowitz, *PLoS One*, 2014, **9**, e88414.
64 M. Alrahili, R. Peroor, V. Savchuk, K. McNear and A. Pinchuk, *J. Phys. Chem. C*, 2020, **124**, 4755–4763.
65 M. Kim, J. H. Lee and J. M. Nam, *Adv. Sci.*, 2019, **6**, 1900471.
66 G. Guan, K. Y. Win, X. Yao, W. Yang and M. Y. Han, *Adv. Healthcare Mater.*, 2021, **10**, 2001158.
67 W. Yang, H. Liang, S. Ma, D. Wang and J. Huang, *Sustainable Mater. Technol.*, 2019, **22**, e00109.
68 L. Chang, X. Liu, J. Zhu, Y. Rao, D. Chen, Y. Wang, Y. Zhao and J. Qin, *Colloids Surf., B*, 2022, **218**, 112747.
69 V. Mulens-Arias, A. Nicolás-Boluda, A. Pinto, A. Balfourier, F. Carn, A. K. Silva, M. Pocard and F. Gazeau, *ACS Nano*, 2021, **15**, 3330–3348.
70 M. Deinavizadeh, A. R. Kiasat, N. Hooshmand, H. I. Labouta, M. Shafiei, M. Sabaeian, R. Mirzajani, S. M. Zahraei, P. Makvandi and M. A. El-Sayed, *ACS Appl. Nano Mater.*, 2023, **6**, 16332–16342.
71 U. A. Awan, A. Raza, S. Ali, R. F. Saeed and N. Akhtar, *Beilstein J. Nanotechnol.*, 2021, **12**, 295–303.
72 A. Mohapatra, J. Mondal, P. Sathiyamoorthy, A. Mohanty, V. Revuri, S. K. Rajendrakumar, Y.-K. Lee and I.-K. Park, *ACS Appl. Mater. Interfaces*, 2023, **15**, 14173–14183.
73 S. Fallah iri sofla, M. Abbasian and M. Mirzaei, *J. Biomater. Sci.*, 2019, **30**, 12–33.
74 F. Zhu, G. Tan, Y. Jiang, Z. Yu and F. Ren, *Biomater. Sci.*, 2018, **6**, 2905–2917.
75 X. Zhang, Y. Liu, L. Luo, L. Li, S. Xing, T. Yin, K. Bian, R. Zhu and D. Gao, *Mater. Sci. Eng., C*, 2019, **101**, 505–512.
76 T. Sun, L. Zhang, S. Xiao, Q. Xie, M. Wang, Y. Zhao, C. Zhou, M. Gong and D. Zhang, *ACS Mater. Lett.*, 2024, **6**, 985–998.
77 W. Zhang, K. Cai, Z. Sun, Q. Xiang, L. Yuan, M. Fu, X. Liu, M. F. F. Foda, Z. Ye and J. Huang, *ACS Nano*, 2023, **17**, 18932–18941.
78 R. Wang, H. Yang, R. Fu, Y. Su, X. Lin, X. Jin, W. Du, X. Shan and G. Huang, *Cancers*, 2020, **12**, 3136.
79 D. Zheng, K. Zhang, B. Chen, N. Zhao and F. J. Xu, *Small*, 2020, **16**, 2002790.
80 A. K. Parchur, G. Sharma, J. M. Jagtap, V. R. Gogineni, P. S. LaViolette, M. J. Flister, S. B. White and A. Joshi, *ACS Nano*, 2018, **12**, 6597–6611.
81 Z. Du, Y. Qi, J. He, D. Zhong and M. Zhou, *Wiley Interdiscip. Rev.: Nanomed. Nanobiotechnol.*, 2021, **13**, e1672.
82 C. Qiu, W. Zhang, Y. Zhou, H. Cui, Y. Xing, F. Yu and R. Wang, *Chem. Eng. J.*, 2023, **459**, 141502.
83 B. Yin, W. K. H. Ho, X. Xia, C. K. W. Chan, Q. Zhang, Y. M. Ng, C. Y. K. Lam, J. C. W. Cheung, J. Wang and M. Yang, *Small*, 2023, **19**, 2206762.
84 Y. Chen, W. Meng, M. Chen, L. Zhang, M. Chen, X. Chen, J. Peng, N. Huang, W. Zhang and J. Chen, *J. Mater. Chem. B*, 2023, **11**, 10003–10018.
85 D. Cheng, J. Gong, P. Wang, J. Zhu, N. Yu, J. Zhao, Q. Zhang and J. Li, *J. Mater. Chem. B*, 2021, **9**, 9316–9323.
86 X. Yan, K. Li, T. Q. Xie, X. K. Jin, C. Zhang, Q. R. Li, J. Feng, C. J. Liu and X. Z. Zhang, *Angew. Chem., Int. Ed.*, 2024, **63**, e202318539.
87 H.-T. D. Bui, Y. Park, Y. M. Jung, S. Y. Chew and H. S. Yoo, *J. Mater. Chem. B*, 2023, **11**, 6961–6974.
88 B. Shan, H. Liu, L. Li, Y. Lu and M. Li, *Small*, 2022, **18**, 2105638.
89 F. Ai, N. Wang, X. Zhang, T. Sun, Q. Zhu, W. Kong, F. Wang and G. Zhu, *Nanoscale*, 2018, **10**, 4432–4441.
90 Y. Qian, F. Chen, M. Wang, Q. Sun, D. Shao and C. Li, *Adv. Opt. Mater.*, 2023, **11**, 2202060.
91 Z. Yang, X. Wang, G. Liang, A. Yang and J. Li, *J. Mater. Chem. B*, 2022, **10**, 518–536.
92 R. Yan, Y. Guo, X. Wang, G. Liang, A. Yang and J. Li, *ACS Nano*, 2022, **16**, 8399–8418.
93 G. Jalani, R. Naccache, D. H. Rosenzweig, L. Haglund, F. Vetrone and M. Cerruti, *J. Am. Chem. Soc.*, 2016, **138**, 1078–1083.

94 K. Grieger, J. L. Jones, S. F. Hansen, C. O. Hendren, K. A. Jensen, J. Kuzma and A. Baun, *Nat. Nanotechnol.*, 2019, **14**, 998–1001.
95 W. Najahi-Missaoui, R. D. Arnold and B. S. Cummings, *Int. J. Mol. Sci.*, 2020, **22**, 385.
96 J. Wang, D. Liang, Z. Qu, I. M. Kislyakov, V. M. Kiselev and J. Liu, *Nanophotonics*, 2020, **9**, 2425–2435.
97 C. Xue, L. Sutrisno, M. Li, W. Zhu, Y. Fei, C. Liu, X. Wang, K. Cai, Y. Hu and Z. Luo, *Biomaterials*, 2021, **269**, 120623.
98 X. Li, W. Bao, M. Liu, J. Meng, Z. Wang, M. Sun, L. Zhang and Z. Tian, *Biomater. Sci.*, 2022, **10**, 5520–5534.
99 S. Dey, S. Chatterjee, A. Patel, N. Pradhan, D. Srivastava, N. Patra, A. Bhattacharyya and D. Manna, *Chem. Commun.*, 2021, **57**, 4646–4649.
100 M.-M. Chen, F.-F. Song, M. Feng, Y. Liu, Y.-Y. Liu, J. Tian, F. Lv and Q.-Q. Zhang, *Colloids Surf., B*, 2018, **167**, 104–114.
101 Q. Long, Y. Yang, F. Liao, H. Chen, D. He, S. Li, P. Li, W. Guo and Y. Xiao, *J. Mater. Chem. B*, 2023, **11**, 8528–8540.
102 L. Du, P. Wang, H. Huang, M. Li, S. Roy, Y. Zhang and B. Guo, *Front. Bioeng. Biotechnol.*, 2023, **11**, 1343694.
103 W. Li, J. Yang, L. Luo, M. Jiang, B. Qin, H. Yin, C. Zhu, X. Yuan, J. Zhang and Z. Luo, *Nat. Commun.*, 2019, **10**, 3349.
104 B. Li, M. Zhao, W. Lai, X. Zhang, B. Yang, X. Chen and Q. Ni, *Angew. Chem., Int. Ed.*, 2023, **62**, e202302676.
105 S. Correa, A. K. Grosskopf, J. H. Klich, H. L. Hernandez and E. A. Appel, *Matter*, 2022, **5**, 1816–1838.
106 Y. Kong, Y. Dai, D. Qi, W. Du, H. Ni, F. Zhang, H. Zhao, Q. Shen, M. Li and Q. Fan, *ACS Appl. Bio Mater.*, 2021, **4**, 7595–7604.
107 Q. Li, J. Cao, Q. Wang, J. Zhang, S. Zhu, Z. Guo and W.-H. Zhu, *J. Mater. Chem. B*, 2019, **7**, 1503–1509.
108 X. Chen, R. Tong, B. Liu, H. Liu, X. Feng, S. Ding, Q. Lei, G. Tang, J. Wu and W. Fang, *Biomater. Sci.*, 2020, **8**, 1380–1393.
109 Y. Zhang, H. Zhou, Z. Zhang, Y. Zhu, T. Wang, L. Yu and H. Song, *Colloids Surf., A*, 2021, **609**, 125662.
110 X. Yang, H. Li, C. Qian, Y. Guo, C. Li, F. Gao, Y. Yang, K. Wang, D. Oupicky and M. Sun, *Nanomed. Nanotechnol. Biol. Med.*, 2018, **14**, 2283–2294.
111 S. Yadav, K. Ramesh, P. Kumar, S.-H. Jo, S. I. Yoo, Y.-S. Gal, S.-H. Park and K. T. Lim, *Materials*, 2021, **14**, 7913.
112 L. Li, X. Liang, T. He, X. Li, X. Huang, N. Wang, M. Shen, Y. Shu, R. Wu and M. Zhang, *Biomaterials*, 2022, **290**, 121815.
113 P. Liu, G. Chen and J. Zhang, *Molecules*, 2022, **27**, 1372.
114 J. Y. Li, Y. H. Feng, Y. T. He, L. F. Hu, L. Liang, Z. Q. Zhao, B. Z. Chen and X. D. Guo, *Acta Biomater.*, 2022, **153**, 308–319.
115 F. Rahmani, R. Atabaki, S. Behrouzi, F. Mohamadpour and H. Kamali, *Int. J. Pharma.*, 2023, **631**, 122484.
116 T. Ci, L. Chen, L. Yu and J. Ding, *Sci. Rep.*, 2014, **4**, 5473.
117 D. Sharma, L. Lipp, S. Arora and J. Singh, *Mater. Biomed. Eng.*, Elsevier, 2019, pp. 449–477.
118 A. Pan, Z. Wang, B. Chen, W. Dai, H. Zhang, B. He, X. Wang, Y. Wang and Q. Zhang, *Drug Delivery*, 2018, **25**, 1495–1503.
119 L. Tang, Q. Xiao, Y. Yin, Y. Mei, J. Li, L. Xu, H. Gao and W. Wang, *Biomater. Sci.*, 2022, **10**, 2370–2383.
120 K. Takahashi, H. Yasui, S. Taki, M. Shimizu, C. Koike, K. Taki, H. Yukawa, Y. Baba, H. Kobayashi and K. Sato, *Bioeng. Transl. Med.*, 2022, **7**, e10388.
121 N. Liu, S. Wu, X. Tian and X. Li, *J. Mater. Chem. B*, 2022, **10**, 5165–5173.
122 Z. Li, N. Song and Y.-W. Yang, *Matter*, 2019, **1**, 345–368.
123 W. Feng, M. Jin, K. Yang, Y. Pei and Z. Pei, *Chem. Commun.*, 2018, **54**, 13626–13640.
124 Q. Wang, P. Zhang, J. Xu, B. Xia, L. Tian, J. Chen, J. Li, F. Lu, Q. Shen and X. Lu, *ACS Appl. Bio Mater.*, 2018, **1**, 70–78.
125 Y.-J. Jo, M. Gulfam, S.-H. Jo, Y.-S. Gal, C.-W. Oh, S.-H. Park and K. T. Lim, *Carbohydr. Polym.*, 2022, **286**, 119303.
126 C. Ruan, C. Liu, H. Hu, X.-L. Guo, B.-P. Jiang, H. Liang and X.-C. Shen, *Chem. Sci.*, 2019, **10**, 4699–4706.
127 C. Liu, X. Guo, C. Ruan, H. Hu, B.-P. Jiang, H. Liang and X.-C. Shen, *Acta Biomater.*, 2019, **96**, 281–294.
128 L. Zhang, X. Guan, X. Xiao, Z. Chen, G. Zhou and Y. Fan, *Eur. Poly. J.*, 2022, **176**, 111424.
129 L. Wang, G. Liu, Y. Hu, S. Gou, T. He, Q. Feng and K. Cai, *Nanoscale*, 2022, **14**, 3097–3111.
130 X. Chen, Z. Wang, X. Sun, Y. Han, Y. Huang, J. Xi, X. Bian, J. Han and R. Guo, *Chem. Eng. J.*, 2021, **403**, 126423.
131 S. Yoo, J. Hou, W. Yi, Y. Li, W. Chen, L. Meng, J. Si and X. Hou, *Sci. Rep.*, 2017, **7**, 1071.
132 L. Wang, K. Liang, X. Jiang, M. Yang and Y. N. Liu, *Chem. – Eur. J.*, 2018, **24**, 6557–6563.
133 L. Zhao, Q. Zou and X. Yan, *Bull. Chem. Soc. Jpn.*, 2019, **92**, 70–79.
134 S. Wang, P. J. Ong, S. Liu, W. Thitsartarn, M. J. B. H. Tan, A. Suwardi, Q. Zhu and X. J. Loh, *Chem. – Asian J.*, 2022, **17**, e202200608.
135 J. Cao, B. Zhu, K. Zheng, S. He, L. Meng, J. Song and H. Yang, *Front. Bioeng. Biotechnol.*, 2020, **7**, 487.
136 A. L. Chin, Y. Zhong and R. Tong, *Biomater. Sci.*, 2017, **5**, 1491–1499.
137 M. Zhao, E. Leggett, S. Bourke, S. Poursanidou, S. Carter-Searjeant, S. Po, M. Palma do Carmo, L. A. Dailey, P. Manning and S. G. Ryan, *ACS Nano*, 2021, **15**, 8790–8802.
138 Y. Wu, H. Wang, F. Gao, Z. Xu, F. Dai and W. Liu, *Adv. Funct. Mater.*, 2018, **28**, 1801000.
139 M. Li, Z. Luo and Y. Zhao, *Chem. Mater.*, 2018, **30**, 25–53.

